Frontiers in Bioscience Landmark

Front. Biosci. (Landmark Ed) **2026**; 31(7): 51871
https://doi.org/10.31083/FBL51871

Original Research

The Ferroptosis-Related Mechanisms of Pentoxifylline in Atrial Fibrillation Treatment

Jia-Bin Zhou[1,†], Zhen-Ye Zhang[1,†], Feng Zhou[1], Tian-Peng Wei[1], Ning Zhao[1], Zhen-Hao Shao[1], Huan-Huan Liu[1], Ying Liu[1], Jun-Xian Shen[1], Dan Wu[1], Yi-Qing Yan[1], Wen-Rui Wang[1], Ling-Ling Qian[1], Ru-Xing Wang[1,*]

[1]Department of Cardiology, the Affiliated Wuxi People's Hospital of Nanjing Medical University, Wuxi People's Hospital, Wuxi Medical Center, Nanjing Medical University, 214023 Wuxi, Jiangsu, China
*Correspondence: ruxingw@njmu.edu.cn (Ru-Xing Wang)
[†]These authors contributed equally.
Academic Editor: Rajesh Katare
Submitted: 13 March 2026 Revised: 21 June 2026 Accepted: 29 June 2026 Published: 17 July 2026

Abstract

Background: Ferroptosis has been increasingly implicated in the pathophysiology of atrial fibrillation (AF). Pentoxifylline (PTX), a methylxanthine derivative, has shown potential therapeutic benefits in cardiovascular diseases; however, its unique role in ferroptosis-associated AF remains unclear. This study aimed to elucidate the molecular mechanisms through which PTX may exert therapeutic effects on ferroptosis-related AF, using a multifaceted approach integrating network pharmacology, bioinformatics, and experimental validation. **Methods:** Two transcriptomic datasets, GSE41177 and GSE79768, were retrieved from the Gene Expression Omnibus (GEO) to identify differentially expressed genes (DEGs) in AF. Ferroptosis-related genes (FRGs) were collected from the FerrDb database. PTX-associated targets were predicted using Super-PRED and SwissTargetPrediction. Overlapping DEGs and predicted PTX targets were intersected with FRGs to identify potential pharmacological targets. Candidate genes were further refined through protein-protein interaction (PPI) network construction and five topological algorithms (Degree, Maximum Neighborhood Component [MNC], Maximal Clique Centrality [MCC], Edge Percolated Component [EPC], and Closeness). Genes exhibiting consistent expression patterns in both GEO datasets were defined as key genes. Diagnostic value was assessed using receiver operating characteristic (ROC) curves. The immune infiltration landscape and correlations with key genes were analyzed via the CIBERSORT algorithm and Spearman correlation. Molecular docking was performed, and PyMOL was used to assess binding affinities between PTX and key gene-encoded proteins. In addition, regulatory networks involving non-coding RNAs and key genes were predicted. Single-cell RNA sequencing (scRNA-seq) was applied to determine cell-type–specific gene expression. Finally, the therapeutic effects of PTX and the underlying ferroptosis-related molecular pathways were evaluated both in an acetylcholine (ACh)-$CaCl_2$-induced AF rat model and in angiotensin II (AngII)-stimulated HL-1 cardiomyocytes. **Results:** From a total of 10,511 DEGs and 315 predicted PTX targets, 87 overlapping pharmacological targets were identified. Thirteen of these overlapped with known FRGs. Among them, *PIK3CA* and *TLR4* emerged as key genes of interest based on PPI network centrality and consistent expression across datasets. Immune profiling revealed significant differences in six immune cell types between AF and control samples, with activated dendritic cells and follicular helper T cells negatively correlated with key gene expression. Molecular docking indicated favorable binding affinities between PTX and both PIK3CA (–4.33 kcal/mol) and TLR4 (–3.72 kcal/mol). Further analysis identified 23 microRNAs (miRNAs) predicted to target PIK3CA and TLR4, of which 21 miRNAs interacted with 22 long non-coding RNAs (lncRNAs), suggesting a complex regulatory network. scRNA-seq analysis revealed enriched PIK3CA expression in mast cells and elevated TLR4 expression in neutrophils and monocytes/macrophages, suggesting involvement of immune-related mechanisms. *In vivo*, PTX significantly reduced AF susceptibility, shortened AF duration, and attenuated atrial structural remodeling. In AngII-stimulated HL-1 cardiomyocytes, PTX markedly suppressed intracellular Fe^{2+} accumulation. In both models, these protective effects coincided with downregulation of TLR4 and upregulation of PIK3CA, implicating modulation of ferroptosis-related pathways as the underlying mechanism. **Conclusions:** This study identifies PIK3CA and TLR4 as pivotal genes in the ferroptosis-associated molecular network of AF and as potential therapeutic targets of PTX. These findings support the potential of PTX to mitigate AF by regulating ferroptosis through these targets, providing a preclinical mechanistic basis for the potential value of PTX in AF management.

Keywords: atrial fibrillation; ferroptosis; pentoxifylline; drug target; molecular docking; single-cell RNA sequencing

1. Introduction

Atrial fibrillation (AF) is the most common form of sustained cardiac arrhythmia, currently affecting approximately 60 million individuals worldwide. Its prevalence is projected to more than double within the next four decades, reflecting a mounting public health concern. AF is marked by chaotic and rapid atrial electrical activity, which compromises ventricular filling and cardiac output, thereby increasing the risk of adverse outcomes such as stroke, heart failure, and premature death. In addition to its clinical burden, AF significantly impairs patients' quality of life and imposes considerable economic costs on healthcare systems [1]. The etiology of AF is multifactorial, involving complex interactions among electrical, structural, and autonomic remodeling of the atria. Contributing risk factors include hypertension, coronary artery disease, valvular abnormalities, and aging [2]. Current treatment options, such as antiarrhythmic pharmacotherapy, electrical cardioversion, and catheter ablation, offer symptom control but fall short of providing a definitive cure, with recurrence and adverse effects remaining substantial challenges [3]. This underscores the urgent need for novel therapeutic strategies guided by a deeper understanding of the molecular mechanisms underpinning AF.

One emerging mechanism thought to underlie cardiovascular pathology is ferroptosis, a regulated form of cell death driven by iron-dependent lipid peroxidation. Ferroptosis is characterized by excessive accumulation of reactive oxygen species (ROS), depletion of glutathione (GSH), inactivation of glutathione peroxidase 4 (GPX4), and catastrophic damage to mitochondria and plasma membranes [4]. The ferroptotic process is controlled through intracellular iron metabolism processes, which include the uptake, storage, and use of iron, together with the tight control of lipid peroxidation [5]. Beyond its established roles in cancer and neurodegenerative diseases, ferroptosis has more recently been implicated in cardiovascular disorders, including heart failure and ischemic injury, suggesting its broader relevance as a potential target for therapeutic intervention in AF [6].

Within the context of AF, dysregulated iron metabolism has been proposed to contribute to arrhythmogenesis by promoting oxidative stress, ion channel remodeling, and disturbances in calcium signaling. Indeed, studies have demonstrated that therapeutic modulation of iron homeostasis using agents such as iron chelators or ferroptosis inhibitors can attenuate AF in iron overload models [7]. Despite these insights, the specific molecular network linking ferroptosis to AF remains poorly delineated, and further research is needed to identify actionable targets and pathways for therapeutic intervention [8].

Pentoxifylline (PTX), a synthetic xanthine derivative, exerts multiple pharmacological effects, including inhibition of phosphodiesterases and subsequent elevation of intracellular cyclic adenosine monophosphate (cAMP) levels [9]. It improves erythrocyte flexibility, reduces blood viscosity, and exerts anti-inflammatory and antioxidant effects, thereby enhancing microvascular perfusion [10]. Clinically, PTX is prescribed for intermittent claudication and other peripheral vascular disorders [11]. While previous studies have explored PTX's role in ischemic heart disease and microcirculatory dysfunction, its therapeutic potential in AF remains largely unexplored, highlighting clear opportunities for further research.

In this study, an integrative bioinformatics framework was employed to uncover the potential role of PTX in regulating ferroptosis-associated pathways in AF and to identify key genes related to this regulatory activity. Public transcriptomic datasets were analyzed to identify differentially expressed genes in AF and cross-referenced with PTX-related targets and known ferroptosis regulators. Key candidate genes were evaluated through network-based screening and immune landscape analysis. To further elucidate PTX's mechanism of action, molecular docking, regulatory RNA interaction mapping, and single-cell transcriptomics were conducted. Finally, *in vivo* experiments using an acetylcholine–calcium chloride–induced AF rat model were performed to validate the effects of PTX on ferroptosis-associated molecular markers, providing a comprehensive foundation for potential therapeutic development.

2. Materials and Methods

2.1 Data Source

The transcriptome data for AF were downloaded from the Gene Expression Omnibus (GEO) database (https://www.ncbi.nlm.nih.gov/geo/). Among them, GSE41177 (HG-U133 Plus 2) was used as the training set, which contained 6 normal atrial tissue samples and 32 AF tissue samples, while GSE79768 (HG-U133 Plus 2) was used as the validation set, including 12 normal atrial tissue samples and 14 atrial fibrillation tissue samples. Single-cell RNA sequencing (scRNA-seq) data from the GSE261170 dataset were also obtained from the GEO database. Subsequent analysis was performed on nine cardiac tissue-derived AF samples within this dataset. PTX drug targets were mined from Super-PRED and SwissTargetPrediction websites. Besides, we collected 564 ferroptosis-related genes (FRGs) from the FerrDb database (http://www.zhounan.org/ferrdb/).

2.2 Acquisition and Enrichment Analyses of Pharmacodynamic Targets

Firstly, the differentially expressed genes (DEGs) between AF and control groups in GSE41177 were identified by the limma (v 3.52.4, Melbourne, Victoria, Australia) package with $|\log_2 FC| > 1$ and adj.p value < 0.05 as screening conditions [12]. The UniProt-numbered drug targets were converted to genes in the Uniport database. Then, the DEGs were intersected with the PTX drug targets after deduplication to obtain pharmacodynamic targets. Af-

ter that, the pharmacodynamic targets were subjected to Gene Ontology (GO) and Kyoto Encyclopedia of Genes and Genomes (KEGG) functional enrichment analysis via the ClusterProfiler (v 4.4.4, Guangzhou, Guangdong, China) package with adj.*p* value < 0.05 [13].

2.3 Identification of Candidate Genes

The candidate genes were identified by taking the intersection of pharmacodynamic targets with FRGs, and their interaction network with PTX was visualized. In addition, protein-protein interaction (PPI) networks of candidate genes were constructed with a threshold = 0.4 in the STRING database (https://string-db.org/) and visualized by Cytoscape (v 3.9.1, San Diego, CA, USA) software [14].

2.4 Screening and Validation of Key Genes

Firstly, five algorithms (Degree, Maximum Neighborhood Component [MNC], Maximal Clique Centrality [MCC], Edge Percolated Component [EPC] and Closeness) in the cytoHubba plug-in for Cytoscape software were applied to screen key genes from candidate key genes with interaction relationships in the PPI network [15]. Next, the top 5 genes in the five algorithms with the highest degree of interaction were intersected to obtain the candidate key genes in this study. Then, the expression of the candidate key genes in GSE41177 and GSE79768 was investigated by the ggplot2 (v 3.3.6, Boston, MA, USA) package [16], and the genes with the same expression trend in the two datasets and significant differences between the AF and control groups were referred to as key genes. Afterwards, receiver operating characteristic (ROC) curves were plotted in GSE41177 and GSE79768 via the pROC package to evaluate the diagnostic performance of key genes [17]. Finally, all genes were ranked according to the correlation between the key genes and the expression of all genes in GSE41177, and the key genes were subjected to gene set enrichment analysis (GSEA) using the clusterProfiler (v 4.4.4) and org.Hs.eg.db (v 3.15.0, Boston, MA, USA) packages, with the thresholds set to |NES| >1, the NOM $p < 0.05$, q < 0.25 [18].

2.5 Immune Infiltration Analysis

Firstly, the infiltration abundance of 22 immune cells in GSE41177 was investigated based on the CIBERSORT algorithm [19]. Then, the differences in immune cell infiltration between the AF and control groups were compared by the rank sum test [20]. Finally. The correlation of key genes with differential immune cells was analyzed by Spearman, which was visualized by the ggcorrplot package [21,22].

2.6 Construction of Key Gene and Drug Networks

Firstly, based on the results of GSEA, the signaling pathways in which the key genes were all involved were used to construct a PTX-key gene-signaling pathway network. Then, the molecular docking was carried out between the key gene and the drug (PTX). Specifically, the tertiary structures of receptors (key genes) and small-molecule drugs were downloaded from the PDB database (http://www.idrtech.com/PDB-Ligand/) and PubChem database (https://pubchem.ncbi.nlm.nih.gov), respectively. After that, the molecular docking was performed via the AutoDock software (San Diego, CA, USA) [23]. Finally, the structures that resulted in lower binding free energies and hydrogen-bonded structures were selected for docking visualization via PyMOL (v 2.6, Portland, OR, USA) [24]

2.7 The Regulatory Network of Key Genes

To investigate the regulatory roles of non-coding RNAs on key genes, miRNAs and lncRNAs associated with key genes were predicted using the Starbase database (https://starbase.sysu.edu.cn/). For miRNA prediction, the following criteria were applied: (1) TDMDScore ≥1, (2) clipExpNum ≥1, and (3) concurrent prediction by microT and PITA algorithms. Subsequently, lncRNAs interacting with these miRNAs were identified based on thresholds of TDMDScore ≥1 and clipExpNum ≥20. Thereafter, a regulatory network, including key genes, miRNA, and lncRNA, was constructed.

2.8 scRNA-Seq Analysis

scRNA-seq data from nine cardiac tissue-derived AF samples were processed from GSE261170 dataset using the Seurat package (v 4.3.0, Satija Lab, New York, NY, USA) [25] in R. Raw expression matrices were imported, and quality control (QC) was rigorously applied to exclude low-quality cells based on the following criteria: (1) Mitochondrial gene content ≤20%; Total unique molecular identifiers (UMIs) per cell <30,000; Detected genes per cell between 200 and 6000 (nFeature_RNA range). Following quality control, the filtered data were log-normalized using the NormalizeData function to mitigate sequencing depth biases. To identify biologically relevant variation, highly variable genes (HVGs) were selected via the vst method implemented in the FindVariableFeatures function. The top 2000 genes exhibiting the highest cell-to-cell variability were retained for downstream principal component analysis (PCA). After that, the percentage of variance explained by each principal component (PC) was ranked, and an elbow plot was generated to determine the optimal number of PCs for downstream clustering. Unsupervised clustering of filtered cells was performed using the FindNeighbors and FindClusters functions (resolution = 0.1), with subsequent visualization using Uniform Manifold Approximation and Projection (UMAP). Cell annotation was implemented based on common marker genes. To assess functional heterogeneity among annotated cell subpopulations, Gene Set Variation Analysis (GSVA) was performed using the gsva package (v 1.44.5, Barcelona, Spain) [26] to calculate enrichment scores for Hallmark gene sets. Then, the

differences in the expression and distribution of key genes in the cells were observed. Cell-cell communication analysis of annotated cell subpopulations was performed with CellChat (v 1.6.1, Irvine, CA, USA) [27], utilizing its embedded CellChatDB resource to evaluate context-specific ligand-receptor crosstalk. Finally, we employed Monocle (v 2.26.0, Seattle, WA, USA) [28] to model pseudotime trajectories of cell subpopulations, enabling systematic interrogation of differentiation pathways and temporal key gene expression patterns.

2.9 Animal Studies and Experimental Design

Sample sizes were calculated using G*Power software (v3.1, Heinrich Heine University Düsseldorf, Germany) based on preliminary data, setting $\alpha = 0.05$ and power = 0.80. Rats were randomized into groups using computer-generated sequences (R v4.2, Vienna, Austria), and investigators were blinded to group allocation during ECG acquisition and data analysis. The primary outcome was AF duration following Ach-$CaCl_2$ provocation. Exclusion criteria comprised failure to establish the AF model (inability to induce AF > 3 s), death prior to data collection, and poor-quality ECG signals.

Male Sprague-Dawley rats (200 ± 20 g), aged 6–8 weeks, were procured from Changzhou Cavens Laboratory Animal Co., Ltd. and housed at the Laboratory Animal Center of Wuxi People's Hospital, affiliated with Nanjing Medical University. The rats had ad libitum access to a standard diet and water, with a 12-hour light-dark cycle maintained at 24 °C and 60% humidity. The Animal Ethics Committee of Wuxi People's Hospital approved all experimental procedures (Approval number: DL2025016). Rats were randomly assigned to three groups: CON, AF and AF + PTX (MedChemExpress, Monmouth Junction, NJ, USA). An AF model was induced via intraperitoneal injection (0.1 mL/100 g) of acetylcholine and $CaCl_2$ (66 μg/mL + 10 mg/mL) once daily for 7 days [29]. On the eighth day, 18 rats were randomly assigned to three groups (n = 6). The AF group received intragastric normal saline (8 mL/kg·d). The AF + PTX group was given PTX intragastrically at 30 mg/kg·d [30]. The control group (CON) also received normal saline intragastrically (8 mL/kg·d). Treatments lasted for two weeks. Post-anesthesia with 3% sodium pentobarbital (40 mg/kg), electrodes were subcutaneously inserted into the limbs and connected to a computer electrocardiogram leads. The BL-420N multi-channel biological function experimental system (Chengdu Taimeng, Chengdu, Sichuan, China) recorded and analyzed electrocardiogram data. Upon successful modeling, electrocardiograms were recorded at rest and following tail vein injection of the Ach-$CaCl_2$. Atrial fibrillation was characterized by f waves and the absence of P waves. Following the terminal experimental procedures, euthanasia was performed under deep surgical anesthesia (induced by the sodium pentobarbital mentioned above) to ensure the animals did not experience pain or distress. The specific method was an intravenous overdose of pentobarbital (200 mg/kg). This method is consistent with the AVMA Guidelines for the Euthanasia of Animals.

2.10 Histological Analysis

Rat atrial tissue samples were fixed overnight in 4% paraformaldehyde phosphate-buffered saline (PBS), sectioned, dehydrated with graded ethanol, cleared with xylene, and embedded in paraffin. The paraffin blocks were then sectioned and mounted on glass slides. Following dewaxing, Masson staining was applied to assess atrial fibrosis. Immunohistochemical staining targeted type I and type III collagen, with positive reactions appearing as brownish-yellow granules. The granule quantity and intensity indicated the expression levels of the target proteins.

2.11 Transmission Electron Microscope

Atrial tissues were initially fixed with 1% glutaraldehyde for 10 minutes, then with 3% glutaraldehyde at room temperature for 1 hour. They were subsequently fixed with 1% osmium tetroxide in 0.1 mol/L cacodylate buffer at room temperature for 1 hour, dehydrated in ethanol, and embedded in resin. Following polymerization, ultrathin sections were counterstained with uranyl acetate and lead nitrate. Mitochondrial morphology and striated muscle arrangement were examined using a transmission electron microscope.

2.12 Determination of MDA and GSH Levels

Malondialdehyde (MDA) levels in atrial tissue were quantified using an MDA detection kit (Nanjing Jiancheng Biotechnology Research Institute, Nanjing, Jiangsu, China), with absorbance measured at 530 nm via a microplate reader. Similarly, reduced GSH levels in atrial muscle tissue were assessed using a GSH detection kit (Nanjing Jiancheng Biotechnology Research Institute, Nanjing, Jiangsu, China), following the manufacturer's protocol. Absorbance was recorded at 405 nm and compared against a standard curve.

2.13 Western Blotting Analysis

Protein samples were extracted from atrial tissues using a protein extraction reagent, and their concentration was determined with a BCA Protein Assay Kit (Vazyme, Nanjing, Jiangsu, China). The samples underwent electrophoresis on a 10% SDS-PAGE (Vazyme, Nanjing, Jiangsu, China) and were transferred to a PVDF membrane. After a 2-hour room-temperature block with 5% non-fat milk, the membrane was incubated overnight at 4 °C with the primary antibody. It was then washed three times with TBST and incubated for 2 hours with the secondary antibody. The bands were developed using a chemiluminescent reagent and analyzed quantitatively with ImageJ software (Bethesda, MD, USA). The following anti-

bodies were used: PIK3CA Antibody (A0265, ABclonal, Wuhan, Hubei, China); TLR4 Antibody (66350-1-Ig, Proteintech, Wuhan, Hubei, China); ACSL4 Antibody (22401-1-AP, Proteintech, Wuhan, Hubei, China); GPX4 Antibody (GB154327, Servicebio, Wuhan, Hubei, China); FTH1 Antibody (11682-1-AP, Proteintech, Wuhan, Hubei, China).

2.14 Cell Culture

Mouse cardiomyocytes (HL-1 cells) were obtained from Shanghai mlbio Biotechnology Co., Ltd. (Shanghai, China). Cells were seeded on pre-coated culture dishes or well plates and maintained in DMEM supplemented with 10% fetal bovine serum at 37 °C in a humidified incubator with 5% CO_2. To model atrial fibrillation-associated injury *in vitro*, cells were stimulated with 1 μM angiotensin II (AngII, MedChemExpress, NJ, USA) for 24 h before analysis [31]. For drug-treatment groups, cells were co-treated with PTX at the indicated concentrations (100 μM). All cell lines were obtained from Shanghai mlbio Biotechnology Co., Ltd. (Shanghai, China) and were authenticated by short tandem repeat (STR) profiling. All cell lines were routinely tested and confirmed to be free of mycoplasma contamination.

2.15 siRNA Transfection

Three siRNAs targeting PIK3CA and a non-targeting control (si-NC) were chemically synthesized. The sequences of si-PIK3CA (5′ to 3′) were GCACAUCUACAACAAGUUATT (#1), CAUGGUGGAUGGACGACAATT (#2), and GGAGAAGCUCAUCAACCUATT (#3). After HL-1 cells adhered to the plate, the most effective siRNA or si-NC was transfected with Lipofectamine 3000 (Invitrogen, Carlsbad, USA) following the manufacturer's instructions. Knockdown efficiency for each siRNA was assessed by western blotting, and the sequence showing the highest silencing efficiency was chosen for subsequent experiments. At 24 h post-transfection, cells were stimulated with 1 μM AngII for an additional 24 h before collection.

2.16 Overexpression Plasmid Transfection

To overexpress TLR4, the full-length TLR4 coding sequence was subcloned into the pcDNA3.1(+) vector to generate the overexpression plasmid (OE-TLR4); the empty vector served as the negative control (OE-NC). After cell adhesion, plasmids were transfected into HL-1 cells using Lipofectamine 3000 (Invitrogen, Carlsbad, USA) according to the manufacturer's protocol. Overexpression efficiency was verified by Western blotting. At 24 h after transfection, cells were treated with 1 μM AngII for an additional 24 h, then harvested for downstream experiments.

2.17 RhoNox-6 Immunofluorescence Staining (Intracellular Fe^{2+} Detection)

Intracellular ferrous iron (Fe^{2+}), a hallmark of ferroptosis, was measured with the RhoNox-6 fluorescent probe (Beyotime Biotechnology, Shanghai, China). After the designated treatments, HL-1 cells were washed with PBS and incubated with RhoNox-6 working solution at 37 °C in the dark for 30 min. Cells were then gently rinsed with PBS to remove unbound probe. Fluorescence images were acquired on a fluorescence or confocal laser-scanning microscope; RhoNox-6 produced red fluorescence proportional to intracellular Fe^{2+}. Mean fluorescence intensity was quantified in ImageJ and reported as a fold change relative to the control group.

2.18 Statistical Analysis

Statistical analyses were conducted using GraphPad Prism 9.3.0 (GraphPad Software, San Diego, CA, USA), with results expressed as mean ± standard error of the mean (SEM). Differences between two groups were assessed using the Student's *t*-test, while one-way analysis of variance (ANOVA) was employed for comparisons among three or more groups, followed by Bonferroni post hoc testing when applicable. A p value of <0.05 was deemed statistically significant.

3. Results

3.1 A Total of 87 Pharmacodynamic Targets Were Screened Out

Firstly, a total of 10,511 DEGs were identified in GSE41177, of which all 10,510 were up-regulated except for 1 gene down-regulated (Fig. 1A,B). Next, a total of 315 drug targets were obtained based on the Super-PRED and SwissTargetPrediction websites (**Supplementary Table 1**). Then, 87 pharmacodynamic targets were obtained by intersecting drug targets with DEGs (Fig. 1C). According to the results of GO enrichment, the signaling pathways enriched for pharmacodynamic targets mainly include response to peptide hormone (biological Process, BP), integral component of presynaptic membrane (Cellular Components, CC), neurotransmitter receptor activity (Molecular functions, MF), etc. (Fig. 1D), while in KEGG, the pharmacodynamic targets are mainly involved in signaling pathways such as neuroactive ligand-receptor interaction, calcium signaling pathway and so on (Fig. 1E).

3.2 A Total of 13 Candidate Genes Were Identified

The intersection of pharmacodynamic targets and FRGs was taken to identify 13 candidate genes (Fig. 2A). In the network of candidate genes-PTX, 13 corresponding relationships were included, such as PTX-SLC2A1, PTX-NFE2L2 and so on (Fig. 2B). In addition, the PPI network of candidate genes indicated that the remaining 12 candidate genes formed 34 relationship pairs except PARP3, for example BRD4-STAT3, PIK3CA-MAPK14 and so on (Fig. 2C).

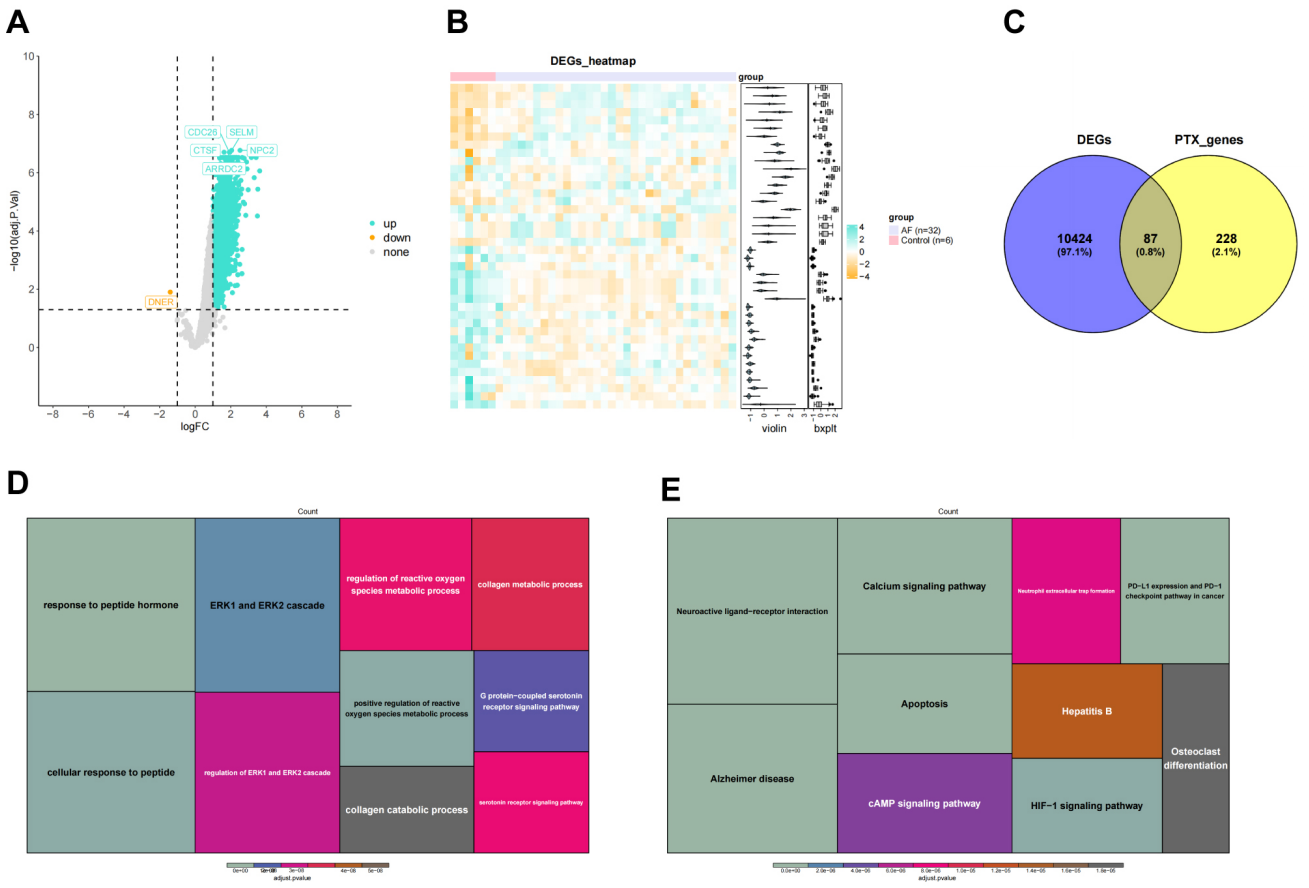

Fig. 1. Bioinformatics analysis of differentially expressed genes and drug targets. (A) Volcano plot of differentially expressed genes (Each dot represents a gene: green indicates upregulated genes, orange indicates downregulated genes, gray indicates non-significant genes). (B) Heatmap of differentially expressed genes (Each column represents a sample; each row shows the expression level of a gene across different samples). (C) Venn diagram of drug-target interactions. (D) Gene Ontology (GO) enrichment analysis of drug targets. (E) Kyoto Encyclopedia of Genes and Genomes (KEGG) pathway enrichment analysis of drug targets.

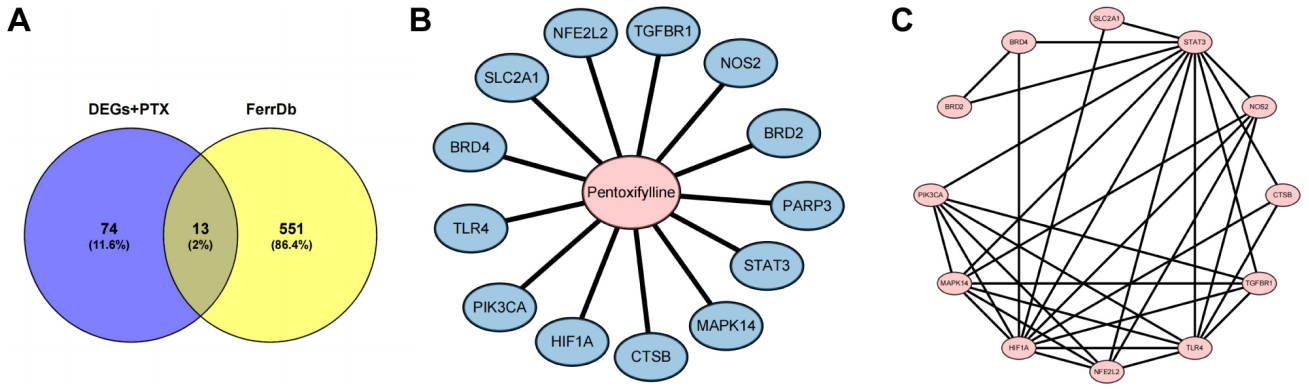

Fig. 2. Screening and interaction networks of candidate genes. (A) Candidate Gene Venn Diagram. (B) Candidate Gene-Pentoxifylline (PTX) Network Construction (Red: Drug; Blue: Candidate Genes). (C) Candidate Gene PPI Network.

3.3 PIK3CA *and* TLR4 *Were Identified as Key Genes for AF Diagnosis*

In this study, Fig. 3A–E showed the top 5 genes with the highest degree of interaction based on Degree, MNC, MCC, EPC and Closeness algorithms, respectively, which were intersected to identify *PIK3CA, TLR4, EGFR, STAT3,* and *HIF1A* as the candidate key genes for the subsequent study (Fig. 3F). Then, *PIK3CA* and *TLR4* were identified as key genes based on the expression of the candidate key genes in GSE41177 and GSE79768, which showed the same expression trend and significant difference between the groups (Fig. 3G,H). The AUC values of ROC curves for

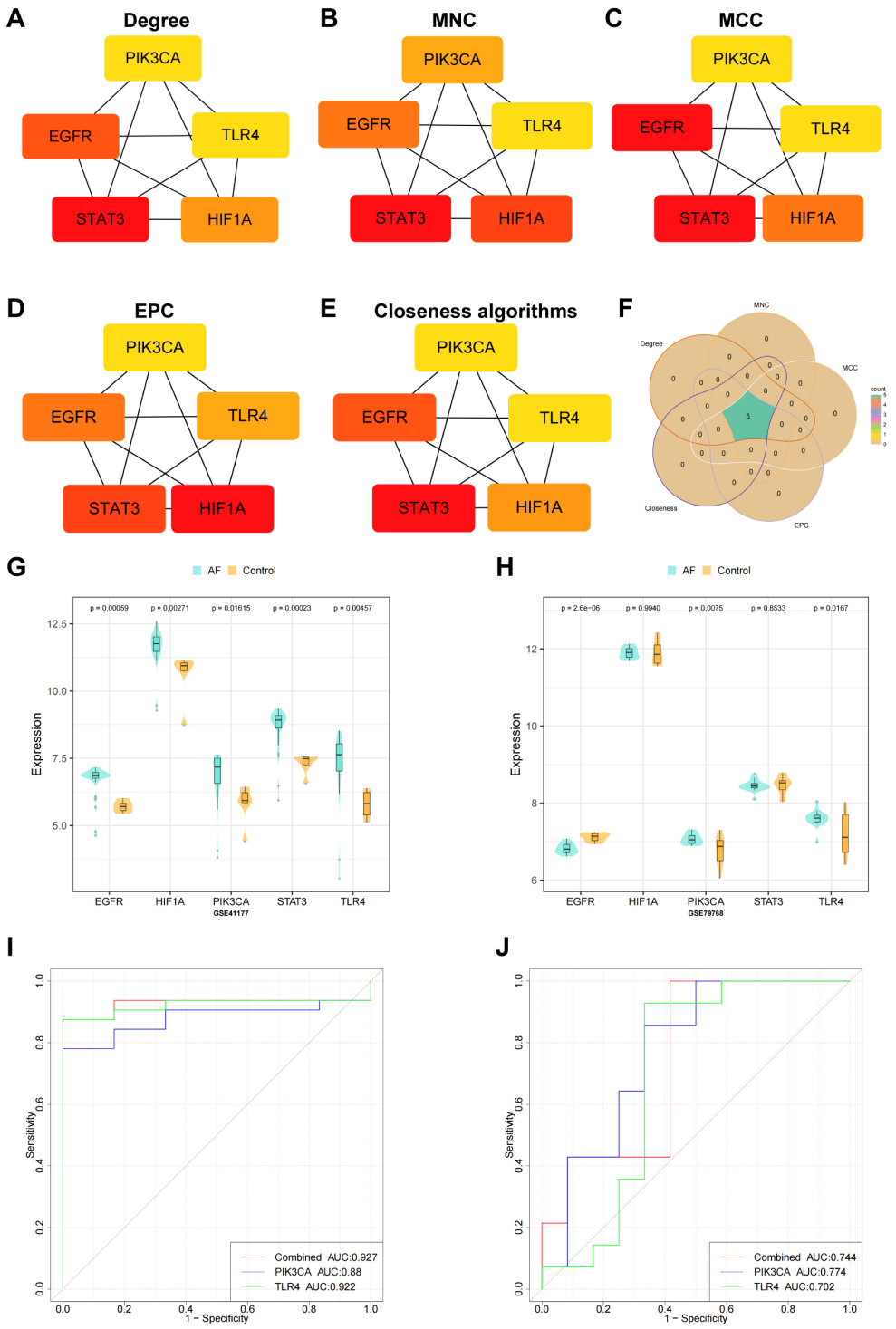

Fig. 3. Identification and validation of key genes using multiple network algorithms. (A) Degree algorithm-based interaction network of top 5 genes (5 nodes, 10 edges; redder color indicates stronger interaction). (B) MNC algorithm-based interaction network of top 5 genes (5 nodes, 10 edges; redder color indicates stronger interaction). (C) MCC algorithm-based interaction network of top 5 genes (5 nodes, 10 edges; redder color indicates stronger interaction). (D) Edge Percolated Component (EPC) algorithm-based interaction network of top 5 genes (5 nodes, 10 edges; redder color indicates stronger interaction). (E) Closeness algorithm-based interaction network of top 5 genes (5 nodes, 10 edges; redder color indicates stronger interaction). (F) Venn diagram of the five algorithms. (G,H) Expression validation of key genes. (I,J) ROC curves of key genes (Left: ROC curve from GSE41177 dataset; Right: receiver operating characteristic (ROC) curve from GSE79768 dataset. "Combined" indicates the diagnostic performance of integrating the two genes).

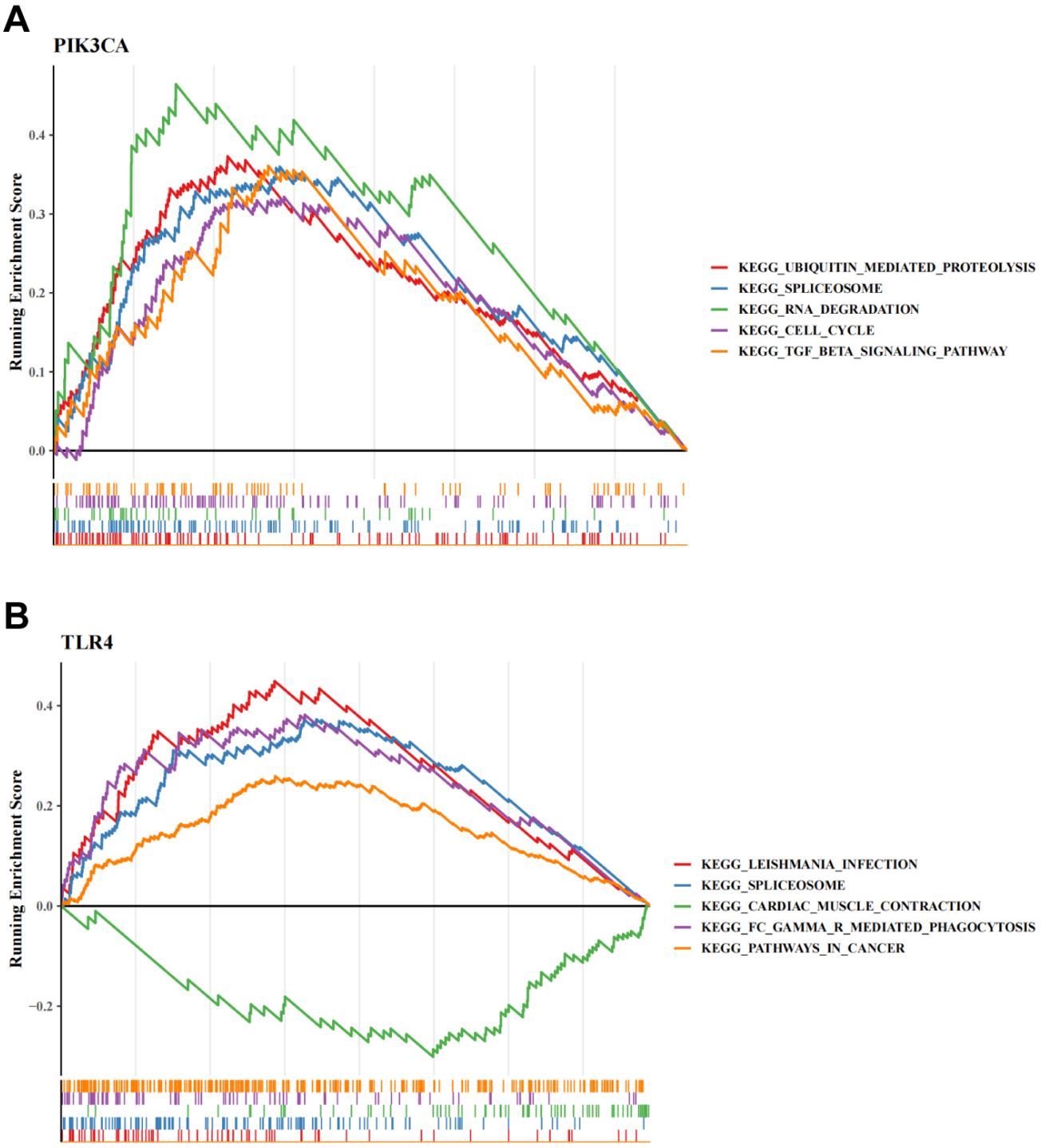

Fig. 4. KEGG pathway enrichment analysis of key genes (PIK3CA and TLR4). (A) KEGG enrichment analysis of the key gene PIK3CA. (B) KEGG enrichment analysis of the key gene TLR4 (Enrichment Score plot: The x-axis represents ranked genes, and the y-axis shows the corresponding Running ES. The peak in the line plot indicates the Enrichment Score (ES) for the functional term gene set. Genes before the peak constitute the core gene set of this pathway. The bottom bar marks genes belonging to the analyzed gene set).

the key genes in GSE41177 and GSE79768 datasets were both greater than 0.7, indicating that they had good diagnostic efficiency for AF (Fig. 3I,J).

Besides, according to the results of GSEA, the signaling pathways enriched by *PIK3CA* mainly include ubiquitin-mediated proteolysis, spliceosome and so on (Fig. 4A), whereas *TLR4* played an important role in leishmania infection, spliceosome, etc (Fig. 4B).

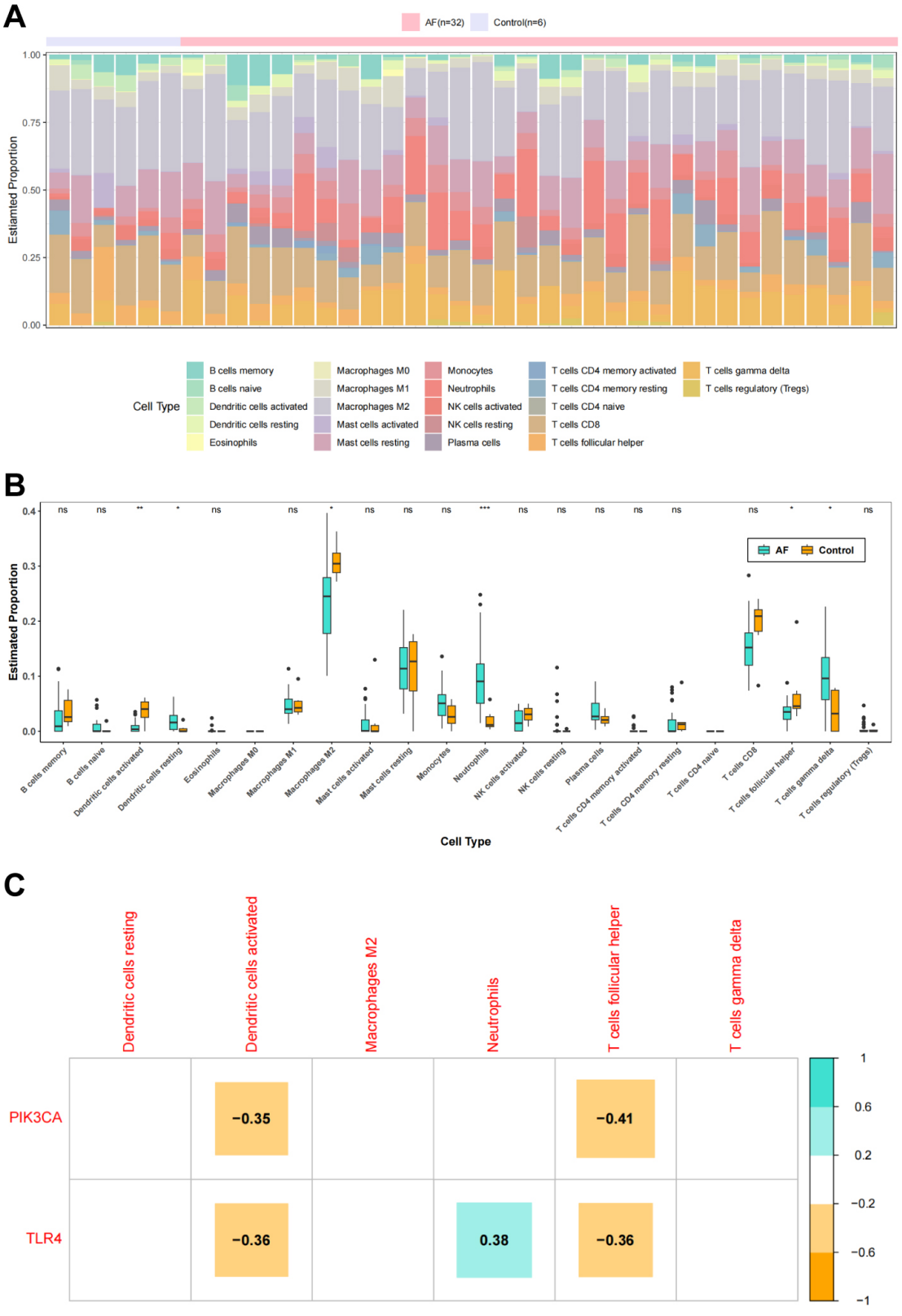

Fig. 5. Immune cell infiltration patterns and their correlation with key genes. (A) Bar chart of immune cell infiltration profiles. (B) Boxplot showing the infiltration levels of 22 immune cell types in disease vs. healthy samples. (C) Correlation analysis between key genes and differentially infiltrated immune cells (Empty cells: non-significant correlation, $p \geq 0.05$; Colored cells: significant correlation, $p < 0.05$. Green hues: positive correlation; orange hues: negative correlation. Darker colors indicate stronger correlations), *: $p < 0.05$; **: $p < 0.01$; ***: $p < 0.001$; ns: not significant.

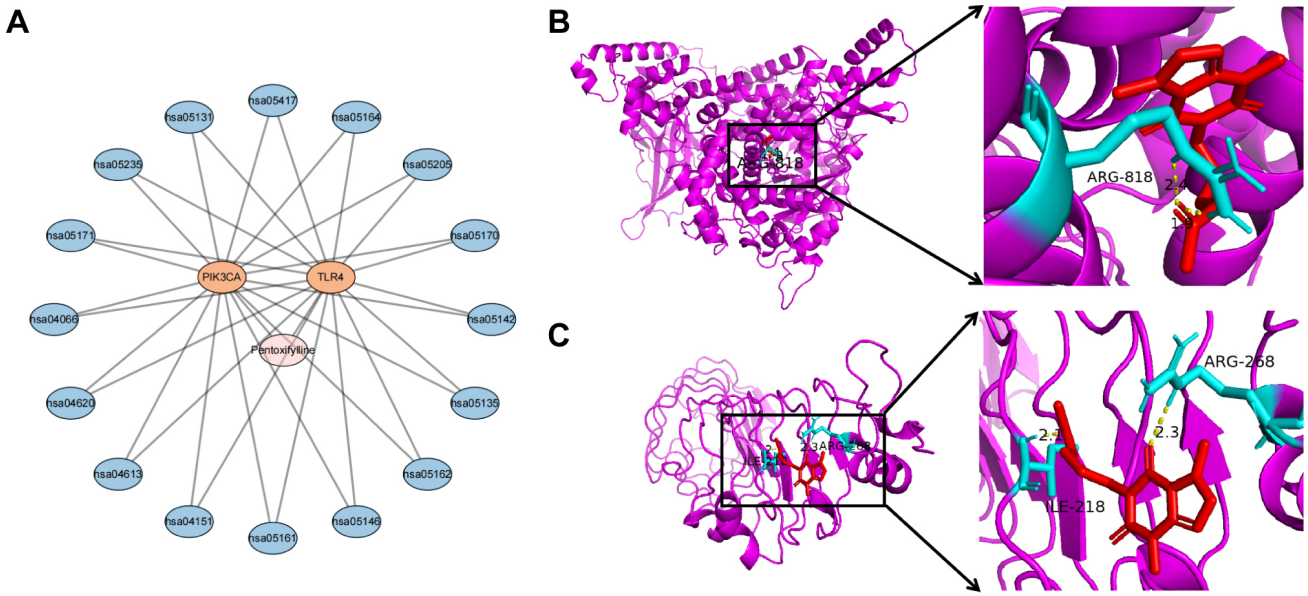

Fig. 6. Network analysis and molecular docking of key targets with pentoxifylline. (A) Drug (PTX)-key gene-pathway network diagram. (B) Molecular docking results of PIK3CA and Pentoxifylline (Note: The red cyclic model represents the active molecule Pentoxifylline. The blue stick structures near Pentoxifylline indicate amino acid residues forming hydrogen bonds with the active molecule. Yellow dashed lines represent hydrogen bonds between the active molecule and amino acid residues. The docking affinity between the active molecule and protein is –4.33 kcal/mol). (C) Molecular docking results of TLR4 and Pentoxifylline (Note: The red cyclic model represents the active molecule Pentoxifylline. The blue stick structures near Pentoxifylline indicate amino acid residues forming hydrogen bonds with the active molecule. Yellow dashed lines represent hydrogen bonds between the active molecule and amino acid residues. The docking affinity between the active molecule and protein is –3.72 kcal/mol).

3.4 The Key Genes Were Negatively Correlated With Activated Dendritic Cells and Follicular Helper T Cells

Firstly, the proportional distribution of the 22 immune cells in GSE41177 can be seen in Fig. 5A. Among them, 6 immune cells, resting dendritic cells, activated dendritic cells, M2 macrophages, neutrophils, follicular helper T cells, and gamma delta T cells, were significantly different between AF and control groups (Fig. 5B). In addition, key genes (*PIK3CA* and *TLR4*) showed significant negative correlations with activated dendritic cells and follicular helper T cells according to Spearman's analysis (Fig. 5C).

3.5 Molecular Docking of PIK3CA, TLR4 and PTX Was Constructed

In this study, 14 signaling pathways in which key genes were jointly involved were used to construct the PTX-key gene-signaling pathway network. This network contained 34 relationship pairs, such as PTX-PIK3CA-hsa05235, PTX-TLR4-hsa05417 and so on (Fig. 6A). Finally, the docking affinity between active molecules and proteins in the docking results of *PIK3CA*, *TLR4* and PTX were –4.33 kcal/mol, –3.72 kcal/mol, respectively (Fig. 6B,C).

3.6 The Molecular Regulatory Mechanism of Key Genes

A total of 23 miRNAs associated with *PIK3CA* and *TLR4* were predicted, among which 21 miRNAs exhibited interactions with 22 lncRNAs (Fig. 7). Specifically, the lncRNAs AL359762.3, AC074117.1, and RNF216P1 were predicted to regulate TLR4 expression via hsa-let-7g-5p, while MALAT1 and XIST modulated PIK3CA through hsa-miR-155-5p.

3.7 The Role of Immune Cells in AF

After integration, 26,627 genes and 80,781 cells were retained (Fig. 8A,B). From these genes, top 2000 HVGs were selected for PCA, and top 30 PCs were chosen for cell clustering (Fig. 8C,D). The cells were clustered into 15 distinct subsets and ultimately annotated as 10 cell types, containing Monocytes/Macrophages, Fibroblasts, T/nature killer (NK) cells, Cardiomyocytes, B cells, Endothelial cells, Neutrophils, Myeloid cell progenitors, Pericytes, and Mast cells (Fig. 8E–G). Enrichment analysis revealed that Monocytes/macrophages and Neutrophils exhibited significant activation of pathways associated with complement and inflammatory response, underscoring their roles in immune dysregulation within AF (Fig. 8H). Gene expression analysis revealed elevated expression of PIK3CA in Mast cells, whereas TLR4 exhibited higher expression levels in Neutrophils and Monocytes/Macrophages, suggesting specific roles for these genes in immune and inflammatory processes (Fig. 8I). Cell communication showed that the interactions between T/NK cells, Monocytes/Macrophages, and fibroblasts and other cells were relatively strong, es-

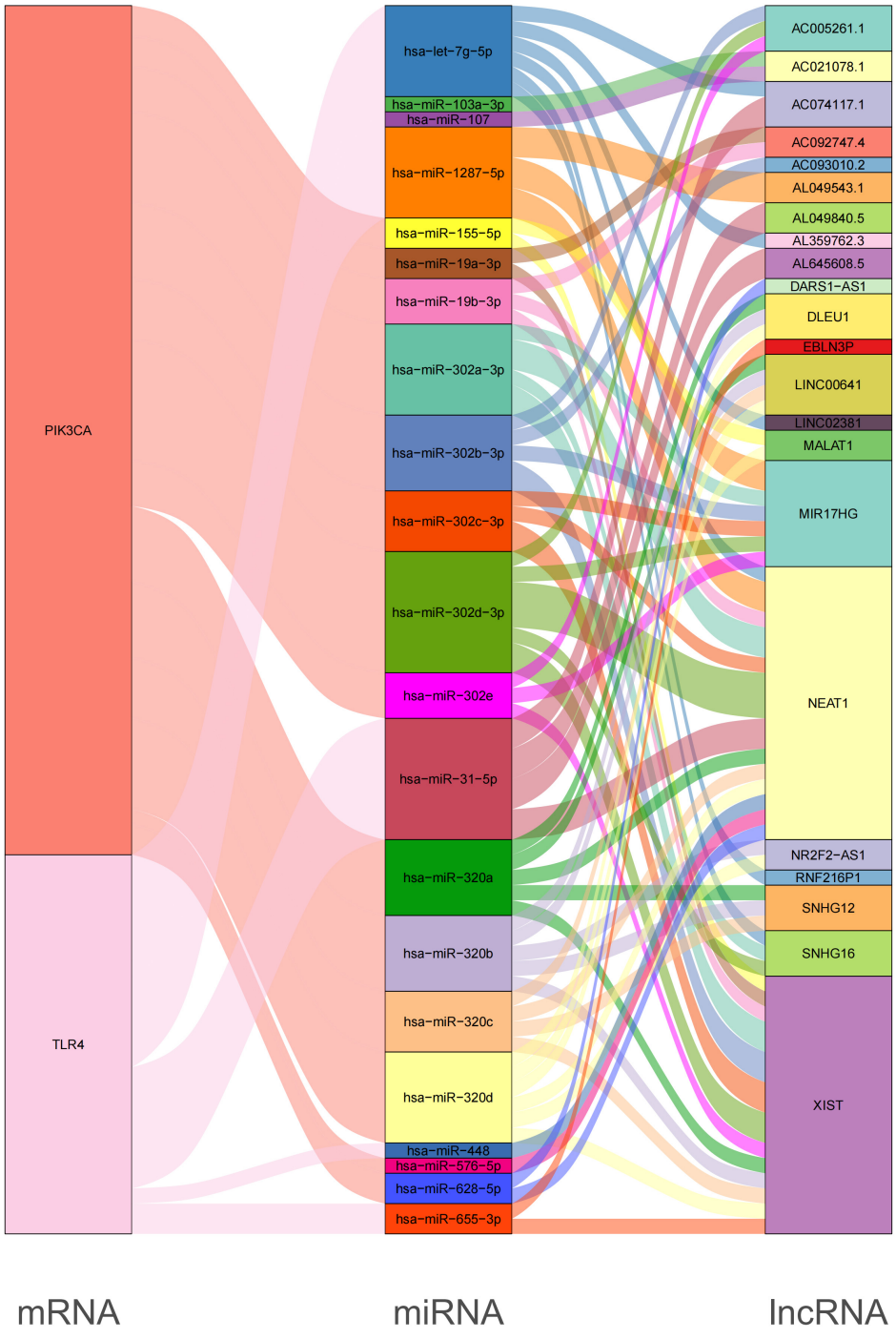

Fig. 7. The regulatory networks of key genes.

pecially between T/NK cells and Monocytes/Macrophages (Fig. 9A). Pseudotemporal trajectory analysis was prioritized for monocytes/macrophages and neutrophils due to the elevated expression of key genes (TLR4 and PIK3CA) in these cell populations and their established roles in the immune response to ferroptosis *in vivo*. Pseudotemporal trajectory analysis revealed distinct expression dynamics for key genes: PIK3CA exhibited no significant temporal variation across both cell lineages, suggesting stable expression throughout differentiation; TLR4 displayed stage-specific regulation in Monocytes/Macrophages, with peak expression during early pseudotime followed by progressive downregulation (Fig. 9B–E).

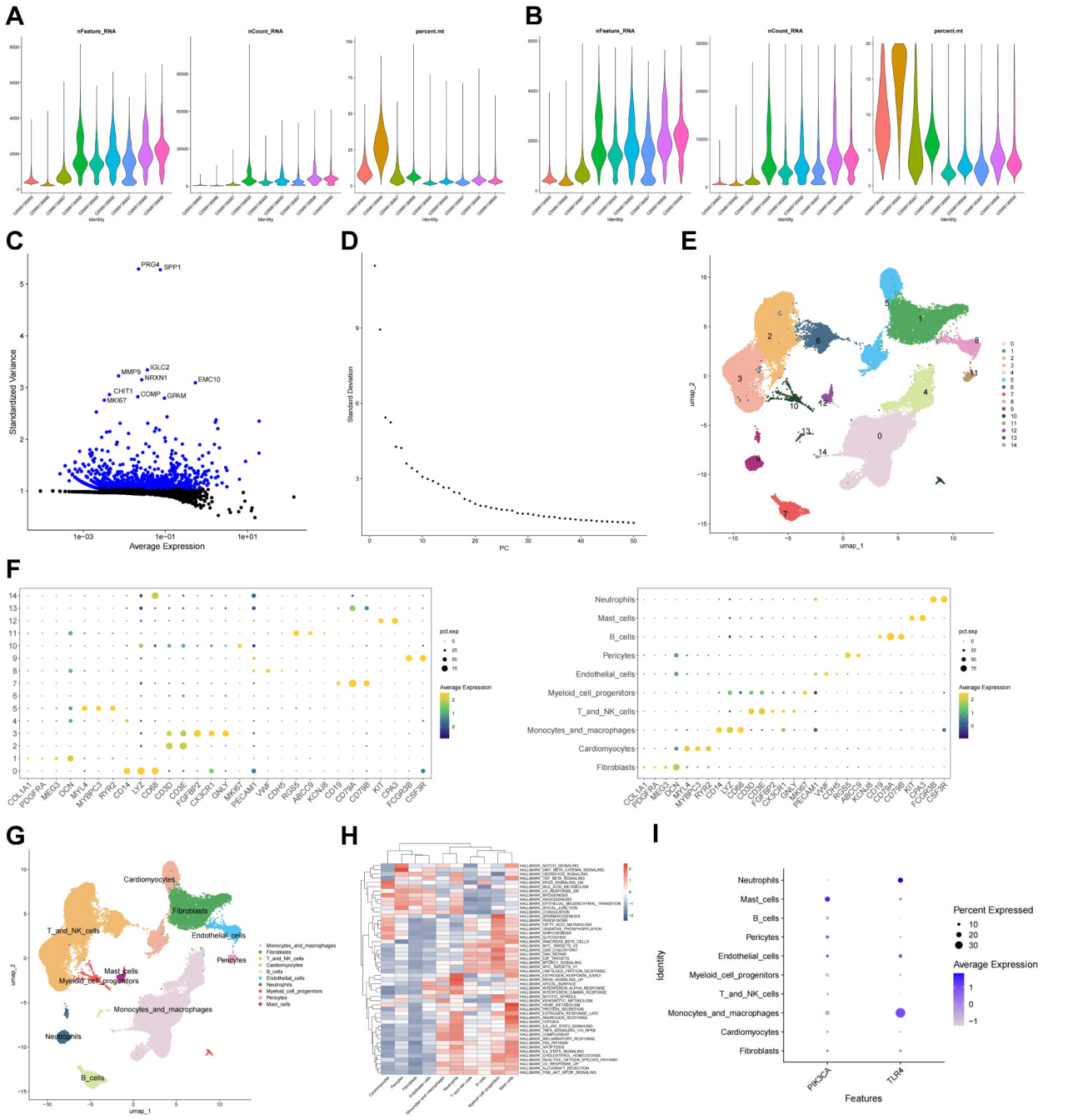

Fig. 8. The expression of key genes in cells. (A) Violin plots illustrating data distribution characteristics before quality control (QC) implementation. (B) Violin plots illustrating data distribution characteristics after QC implementation. (C) Selection of highly variable genes. (D) Elbow chart of PCs. (E) Uniform Manifold Approximation and Projection (UMAP) plot of cells after clustering. (F) Expression of marker gene in cell subsets. (G) UMAP plot after cell annotation. (H) Heat map of cell type enrichment pathways. (I) Dot plot of key genes expression in cell types.

3.8 Pentoxifylline Alleviates Ferroptosis-Associated Atrial Fibrillation in Animal and Cellular Models

We induced AF in rats by continuous intraperitoneal injection of an ACh–$CaCl_2$ mixture for one week, then treated animals with PTX. AF induction was verified by loss of the P wave and appearance of f waves on the electrocardiogram. Programmed electrical stimulation readily elicited AF in the model group but not in controls, and AF induction was substantially reduced in the AF + PTX group (Fig. 10A). PTX treatment significantly decreased AF inducibility (Fig. 10B) and shortened AF duration (Fig. 10C) compared with untreated AF animals. These results indicate that PTX reduces both the occurrence and susceptibility to AF.

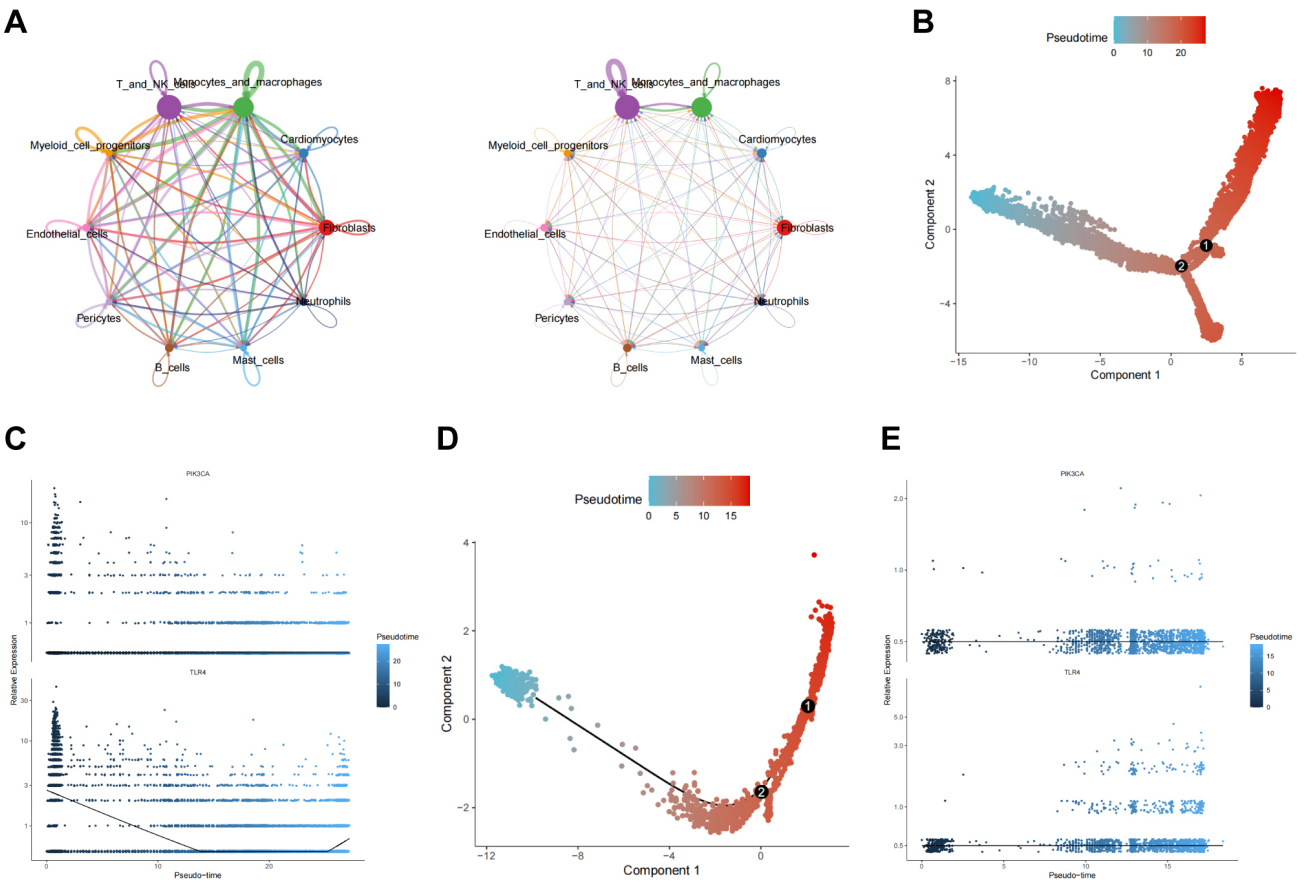

Fig. 9. Results of cell communication and pseudotime trajectory analysis. (A). Results of cell communication. (B) Time trajectories of monocytes/macrophages. (C) The temporal changes of key gene expression in monocytes/macrophages. (D) Time trajectories of neutrophils. (E) The temporal changes of key gene expression in neutrophils.

AF is closely linked to atrial interstitial fibrosis, which drives structural remodeling and sustains arrhythmia. We assessed interstitial fibrosis by Masson staining, in which collagen fibers stain blue and atrial myocytes red. The AF group showed a marked increase in atrial fibrosis with pronounced fiber-induced tissue separation, whereas these changes were notably ameliorated in the AF + PTX group (Fig. 10D). Quantitative analysis confirmed a significantly larger fibrotic area in the AF group that was reduced by PTX (Fig. 10E). We then used immunohistochemistry to evaluate collagen I and collagen III, two canonical fibrosis markers. Both collagen I and collagen III were significantly elevated in the AF group compared with controls, and both were significantly attenuated by PTX (Fig. 10F,G). Together, these findings indicate that PTX effectively suppresses atrial fibrosis in AF rats.

Transmission electron microscopy examined mitochondrial ultrastructure in atrial myocytes. In the AF group, mitochondria were markedly smaller and disorganized, with blurred or absent cristae and ruptured outer membranes which are features characteristic of ferroptosis. In the AF + PTX group, cristae were more abundant and outer-membrane rupture was substantially reduced (Fig. 11A), and the proportion of damaged mitochondria, which was significantly increased in the AF group, was lowered by PTX (Fig. 11B). We then measured oxidative stress and lipid peroxidation markers in atrial tissue. GSH levels were significantly decreased in the AF group and partially restored by PTX (Fig. 11C), whereas MDA levels were significantly elevated in the AF group and reduced after PTX treatment (Fig. 11D). Consistent with ferroptosis, western blotting showed that the pro-ferroptotic marker ACSL4 was upregulated in the AF group and downregulated by PTX, while the anti-ferroptotic markers GPX4 and FTH1 were downregulated in the AF group and restored by PTX (Fig. 11E,F). Together, these findings indicate that PTX inhibits ferroptosis in atrial myocytes of AF rats.

Finally, we experimentally validated the key PTX targets for AF treatment that were identified by bioinformatics analysis. In atrial tissue, both PIK3CA and TLR4 were upregulated in the AF group relative to controls; after PTX treatment, PIK3CA expression increased further, while TLR4 expression decreased significantly (Fig. 11G,H). The same regulatory pattern appeared in AngII-stimulated cardiomyocytes: AngII elevated PIK3CA and TLR4, and PTX further raised PIK3CA while lowering TLR4 (Fig. 12A–

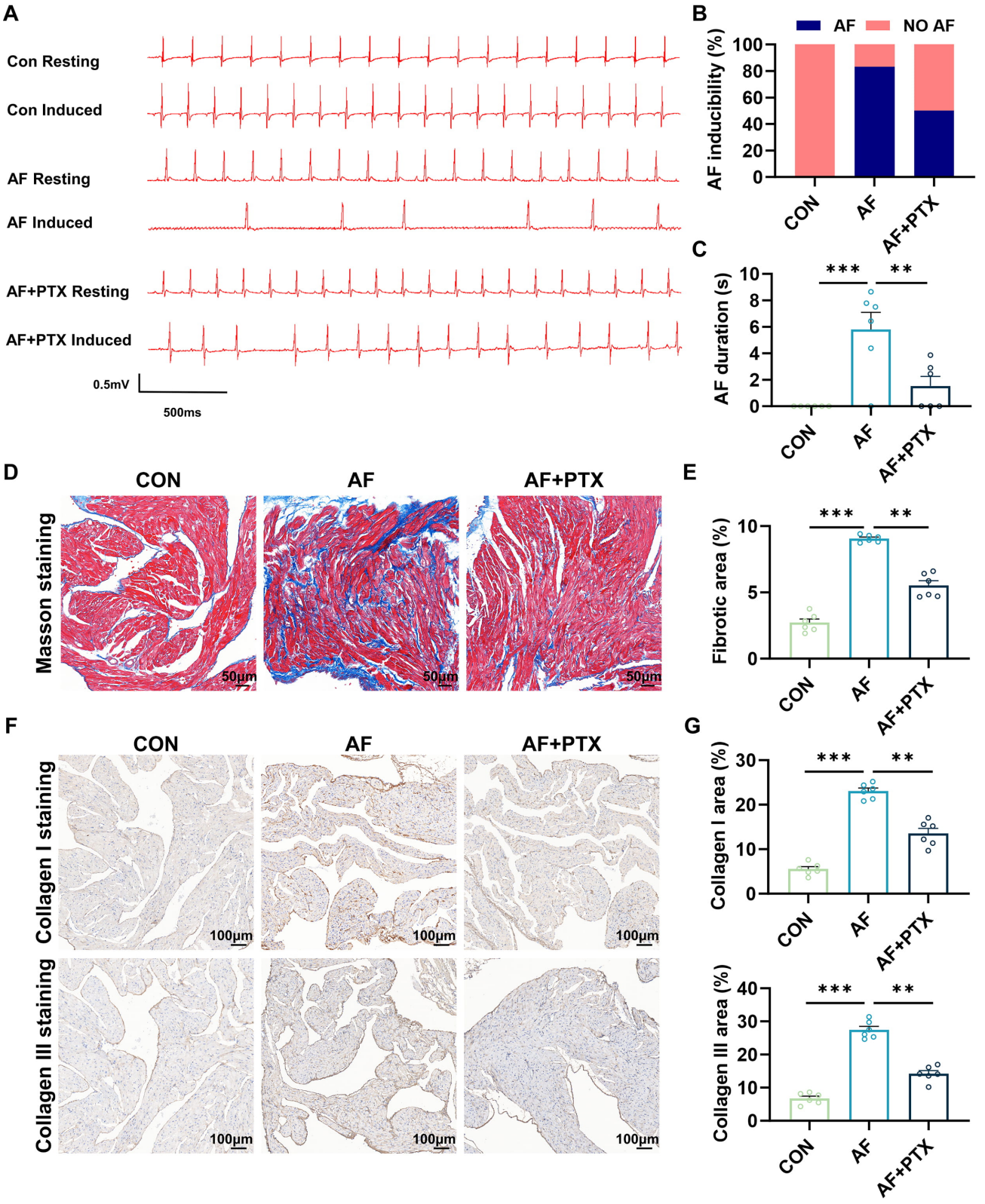

Fig. 10. Animal experiment verification of the protective effect of pentoxifylline in atrial fibrillation. (A) Representative segment of resting electrocardiogram recording. (B,C) Incidence and duration of AF in drug-induced state in each group. (D) Atrial cardiomyocyte fibrosis was detected and quantified via Masson's trichrome staining, scale bar = 50 μm. (E) Quantification of the fibrotic area (%) based on Masson's trichrome staining. (F) Representative immunohistochemical staining for Collagen I and Collagen III in atrial tissue, scale bar = 100 μm. (G) Quantification of the Collagen I–positive area (%) and Collagen III–positive area (%). N = 6/group. Data are means ± SEM. $^{**}p < 0.01$ and $^{***}p < 0.001$.

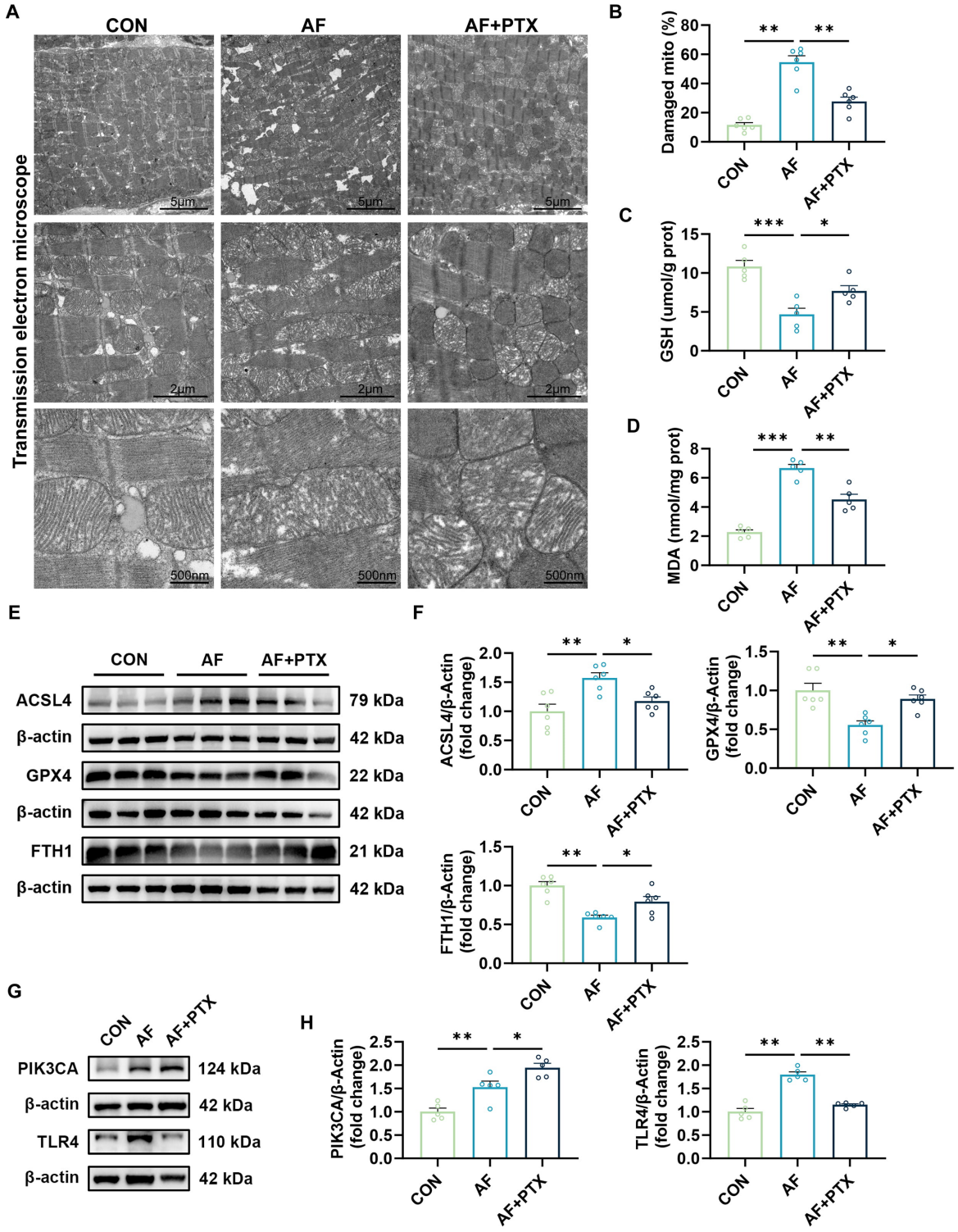

Fig. 11. Animal experiment verification of pentoxifylline on ferroptosis in atrial fibrillation. (A). Transmission electron microscopy was used to examine the ultrastructural morphology of atrial cardiomyocytes. Representative images show distinct pathological alterations across the CON, AF, and AF+PTX groups. Scale bars: 5 μm (top row), 2 μm (middle row), and 500 nm (bottom row). (B) Quantification of the proportion of damaged mitochondria (%) based on TEM analysis. (C,D) Glutathione (GSH) and malondialdehyde (MDA) levels in atrial cardiomyocytes were quantified with appropriate commercial kits. (E) Representative Western blots of the ferroptosis-related proteins ACSL4, GPX4, and FTH1 in atrial tissue. (F) Quantification of ACSL4, GPX4, and FTH1 protein levels, normalized to β-actin and expressed as fold change. (G,H) Representative Western immunoblots with corresponding quantification assessing PIK3CA and TLR4 levels in atrial cardiomyocytes. N = 6/group. Data are means ± SEM. *$p < 0.05$, **$p < 0.01$ and ***$p < 0.001$.

C). To establish causality, we measured intracellular ferrous iron (Fe^{2+}) accumulation using RhoNox-6 staining. AngII markedly increased Fe^{2+} levels, and PTX strongly suppressed that accumulation in the si-NC and OE-NC groups (Fig. 12D–G). Importantly, the protective effect of PTX was largely reversed by PIK3CA knockdown (si-PIK3CA; Fig. 12D,E) and by TLR4 overexpression (OE-TLR4; Fig. 12F,G), with Fe^{2+} accumulation significantly restored relative to the respective negative controls. These findings indicate that PTX inhibits ferroptosis in atrial myocytes via the PIK3CA/TLR4 signaling axis, thereby mitigating AF progression.

4. Discussion

AF is the most common form of sustained cardiac arrhythmia, presenting a complex pathophysiological profile and contributing significantly to cardiovascular morbidity and mortality worldwide [32]. Recent research has implicated ferroptosis, an iron-dependent, non-apoptotic form of regulated cell death, in the initiation and progression of AF [33]. PTX, as a drug with broad pharmacological effects, has shown therapeutic promise in cardiovascular disorders, although its mechanisms in AF remain insufficiently characterized. In the present study, an integrated strategy combining network pharmacology, bioinformatics, and experimental validation was employed to elucidate how PTX may attenuate ferroptosis-related pathways in AF. These analyses identified PIK3CA and TLR4 as central mediators of this regulatory process. Molecular docking confirmed favorable binding interactions between PTX and these targets, and *in vivo* experiments further demonstrated that PTX suppresses ferroptosis in a rat model of AF, providing a mechanistic rationale for its cardioprotective potential.

PIK3CA encodes the catalytic subunit p110α of class IA phosphatidylinositol 3-kinase (PI3Kα), which partners with the regulatory subunit p85α to mediate essential cellular processes, including proliferation, differentiation, and survival [34]. Transcriptomic profiling by Sun et al. [35] in patients with paroxysmal AF revealed significant enrichment of the PI3K/Akt signaling axis, underscoring its relevance in AF pathogenesis. Interestingly, both hypoactivation and hyperactivation of PI3Kα have been linked to AF through divergent mechanisms, indicating the necessity of balanced signaling. Ezeani and Prabhu [36] demonstrated that overexpression of PI3K (p110α) drives atrial and ventricular hypertrophy, potentially through aberrant activation of downstream pathways such as Akt/mTOR and β-catenin, leading to structural remodeling and arrhythmogenicity. Similarly, Li et al. [37] highlighted the role of transforming growth factor-β (TGF-β) in activating PI3K/Akt signaling during cardiac fibrosis, a hallmark of AF. In contrast, PI3K deficiency in murine models, as shown by Bass-Stringer et al. [38], promotes cardiac dysfunction, increased fibrosis, and enhanced vulnerability to thrombotic events and atrial dilation, illustrating its dual-edged influence.

Importantly, the PI3K/Akt axis has also been implicated in the regulation of ferroptosis. In cardiotoxicity models involving the co-administration of Lapatinib and Doxorubicin, Sun et al. [39] identified PI3K/Akt pathway suppression as a critical event leading to oxidative injury and ferroptosis. Conversely, Matrine, which is a known activator of PI3K/Akt, was shown to attenuate LPS-induced ferroptotic damage in cardiac cells [40]. Ye et al. [41] provided mechanistic insight by demonstrating that downregulation of PI3K/Akt impairs nuclear translocation of Nrf2, resulting in reduced expression of antioxidant enzymes such as HO-1 and GPx4. This impairment enhances lipid peroxidation and promotes mitochondrial damage via VDAC1 oligomerization, central to ferroptotic cell death. Pharmacological activation using the PI3K agonist 740Y-P was shown to reverse these effects, supporting a protective role for this signaling pathway.

The present data support these findings, as PIK3CA expression was significantly elevated in myocardial tissues from both AF patients and an AF rat model induced by acetylcholine and calcium chloride. Gene Set Enrichment Analysis (GSEA) indicated that PIK3CA was strongly associated with the ubiquitin-mediated proteolysis pathway, suggesting regulatory control at the post-translational level. Notably, the protein stability of PI3Kα is influenced by polyubiquitination mediated by NEDD4L and TRAF6, the former of which facilitates proteasomal degradation [42], while the latter promotes non-degradative ubiquitination that sustains PI3K/Akt signaling [43]. The present molecular docking results revealed a binding free energy of –4.33 kcal/mol between PTX and PI3Kα, supporting a strong interaction. This suggests that PTX may modulate PI3K/Akt signaling by stabilizing PI3Kα through interference with its ubiquitination dynamics [44,45]. Moreover, prior studies have shown that PTX enhances PI3K/Akt signaling and reduces oxidative stress in testicular ischemia models, promoting cell survival [46]. We hypothesize that PTX exerts a similar effect in cardiomyocytes, activating PIK3CA to counteract ferroptosis and thereby limiting AF-associated structural remodeling. These findings point to a novel cardioprotective mechanism for PTX, offering a potential "dual-regulatory" role in modulating PI3K signaling and preserving myocardial function. Future studies are warranted to define the precise molecular events by which PTX modulates this axis in the context of AF, providing the theoretical basis needed for further therapeutic development. It is noteworthy that the GSE41177 dataset demonstrated a highly asymmetrical upregulation of genes. This transcriptional signature aligns with several independent peer studies analyzing the same cohort, which consistently reported that AF-related DEGs in persistent valvular left atrial tissues are heavily biased toward upregulation [47]. This phenomenon reflects a pervasive and globally coordinated transcriptional activation of pro-fibrotic, inflammatory, and tissue-remodeling cascades in long-standing persistent AF

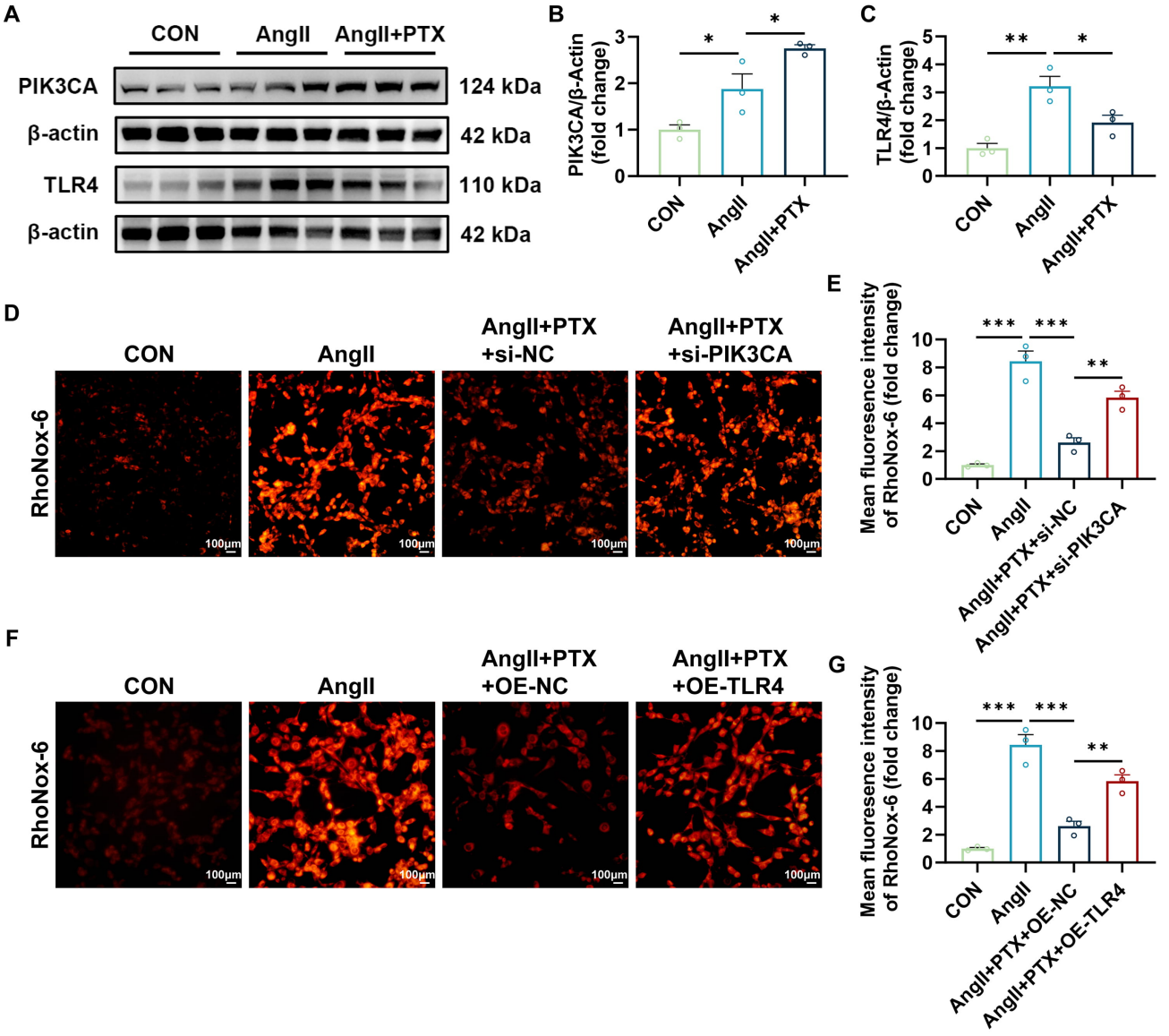

Fig. 12. Cellular experiment verification in HL-1 cardiomyocytes that pentoxifylline alleviates Ang II–induced ferrous iron accumulation via the PIK3CA/TLR4 axis. (A) Representative Western blots of PIK3CA and TLR4 in HL-1 cells. (B,C) Quantification of PIK3CA and TLR4 protein levels, normalized to β-actin and expressed as fold change. (D) Representative fluorescence images of intracellular labile ferrous iron (Fe^{2+}) detected by the RhoNox-6 probe (red) in HL-1 cells from the CON, Ang II, Ang II + PTX + si-NC, and Ang II + PTX + si-PIK3CA groups, scale bar = 100 μm. (E) Quantification of the mean RhoNox-6 fluorescence intensity (fold change relative to CON) corresponding to (D). (F) Representative RhoNox-6 fluorescence images (red) of intracellular Fe^{2+} in HL-1 cells from the CON, Ang II, Ang II + PTX + OE-NC, and Ang II + PTX + OE-TLR4 groups, scale bar = 100 μm. (G) Quantification of the mean RhoNox-6 fluorescence intensity (fold change relative to CON) corresponding to (F). N = 3/group. Data are means ± SEM. *p < 0.05, **p < 0.01 and ***p < 0.001.

rather than a technical preprocessing artifact [48], further validating the biological significance of the identified hub genes.

TLR4, a member of the TLR innate immune receptor family, is expressed on cardiomyocytes and various immune cells and plays a pivotal role in cardiac inflammation and injury. Elevated TLR4 activity has been documented in multiple myocardial pathologies, including ischemia-reperfusion injury, myocarditis, and infarction. Liang et al. [49] reported that fibromodulin (FMOD) activates the TLR4/nod-like receptor protein 3 (NLRP3) inflammasome pathway in spontaneously hypertensive rats, exacerbating atrial fibrosis and inflammatory signaling during AF. Gurses et al. [50], using flow cytometry, found significantly increased TLR4 expression in monocytes of patients with AF, reinforcing its clinical relevance. Likewise, Shuai et al. [51] demonstrated that myeloid differentiation protein 1 (MD1) amplifies atrial inflammation through

TLR4/nuclear factor kappaB (NF-κB) signaling in a high-fat diet-induced AF model, promoting fibrosis and arrhythmogenic substrate development. Supporting these observations, Kong et al. [52] linked gut microbiota dysbiosis to enhanced lipopolysaccharide (LPS) levels, which activate the TLR4/NF-κB/NLRP3 inflammasome axis, contributing to AF via ferroptotic mechanisms and structural remodeling of atrial tissue.

Researchers have shown that silencing TLR4 significantly suppresses both autophagy and ferroptosis in cardiomyocytes derived from heart failure models. This inhibition is likely mediated via p53, a downstream effector of TLR4 signaling, which acts as a transcriptional repressor of SLC7A11 and GPX4. The resulting downregulation of these genes impairs glutathione synthesis and enhances lipid peroxidation, thereby accelerating ferroptosis [53]. The TLR4/NF-κB signaling cascade, a key component of the innate immune response, is known to be involved in multiple aspects of cardiovascular disease, including myocardial ischemia, structural remodeling, fibrosis, and heart failure [54]. Chen et al. [55] demonstrated that heat shock can activate TLR4/NF-κB signaling in cardiomyocytes, leading to increased ferroptosis, while pharmacological inhibition of TLR4 using TAK-242 or NF-κB using PDTC reduces ferroptotic cell death. Moreover, ferroptosis contributes to a self-propagating inflammatory loop by releasing damage-associated molecular patterns (DAMPs), which in turn activate TLR4. This stimulates either NF-κB signaling or NLRP3 inflammasome activation, resulting in elevated secretion of pro-inflammatory cytokines such as IL-1β and IL-18 [56,57]. Such feedback mechanisms amplify inflammation and are implicated in the pathological progression of cardiac disease.

In this study, bioinformatic analyses revealed for the first time a marked upregulation of TLR4 in the myocardial tissues of patients with AF, with its expression positively correlated with multiple ferroptosis-related genes. GSEA further indicated that TLR4 is highly enriched in pathways associated with Leishmania infection, reflecting its fundamental role in mediating inflammatory responses. Prior work has shown that inhibition of TLR4 significantly attenuates inflammation [58]. Our molecular docking analyses demonstrated a strong binding affinity between PTX and TLR4. Consistent with these findings, *in vivo* experiments indicated that PTX may suppress TLR4-mediated ferroptosis and inflammatory responses by directly targeting TLR4. These results support a novel mechanistic framework wherein PTX mitigates AF pathophysiology by interrupting the TLR4/NF-κB signaling axis [59,60]. This suppression of ferroptosis-driven myocardial injury and structural remodeling provides a potential therapeutic avenue for AF management. However, further *in vitro* validation is required to elucidate the precise regulatory effects of PTX on the TLR4 pathway, laying the groundwork for the rational design of new anti-AF agents.

Notably, the scRNA-seq analyses conducted herein revealed cell-type-specific patterns of PIK3CA and TLR4 expression. PIK3CA was predominantly upregulated in mast cells, implicating it in PI3K-Akt signaling cascades relevant to innate immune activation. TLR4 expression, on the other hand, was elevated in neutrophils and monocyte/macrophage populations, consistent with their known roles in pathogen detection and cytokine secretion. These findings suggest that the cell-specific expression of PIK3CA and TLR4 contributes to immune dysregulation in the AF microenvironment. This dysregulation may potentiate both TLR4-mediated NF-κB activation and PI3K-driven survival pathways, thus sustaining a pro-inflammatory and pro-fibrotic milieu. Under homeostatic conditions, mast cells are resident within cardiac tissue and contribute to immune surveillance and tissue maintenance. However, patients with cardiomyopathies show a notable increase in mast cell density in the myocardium [61]. Hyperglycemia is known to enhance mast cell activation, promoting inflammation and fibrosis through the TGF-β/Smad3 signaling axis, ultimately fostering a substrate favorable for arrhythmogenesis [62]. The mast cell-enriched expression of PIK3CA likely augments these effects via persistent activation of the PI3K-Akt pathway, promoting cell survival and facilitating the secretion of inflammatory mediators. Interventions targeting the mast cell/PDGF-A signaling axis could interrupt this pathogenic feedback loop and may offer novel preventive strategies for stress-induced AF. In parallel, recent investigations have identified an expansion of monocyte and macrophage populations in patients with AF, a finding replicated in animal models through histological and single-cell transcriptomic analyses [63]. Large-scale clinical studies have further identified a prominent role for CD14++CD16+ intermediate monocytes in AF development, suggesting a shift in the immune profile of the left atrium [64]. These myeloid cell subsets, characterized by elevated TLR4 expression, likely contribute to fibrotic remodeling via sustained activation of the TLR4-NF-κB axis, thereby promoting collagen deposition and electrical instability. Furthermore, neutrophil extracellular traps (NETs) have been implicated in AF pathogenesis by inducing mitochondrial depolarization and ROS accumulation, triggering autophagy and apoptosis in cardiomyocytes. Pharmacological inhibition of NETosis has been shown to significantly reduce myocardial fibrosis associated with AF [65,66]. The elevated expression of TLR4 in neutrophils and monocytes/macrophages mechanistically aligns with enhanced NET formation, suggesting a feed-forward loop in which TLR4 activation promotes NETosis, thereby amplifying inflammatory and fibrotic responses. These mechanistic insights further support the proposed dual action of PTX in attenuating AF by simultaneously modulating PIK3CA- and TLR4-related pathways, ultimately disrupting pathological immune and fibrotic remodeling.

5. Limitations

Several limitations of this study merit acknowledgment. First, the atrial fibrillation model was induced by intraperitoneal administration of an ACh-$CaCl_2$ mixture, an established acute, inducible model suited primarily to assess AF susceptibility and inducibility. This paradigm does not capture the complex, multifactorial substrate progression that characterizes human AF, particularly persistent forms and the chronic remodeling associated with aging, hypertension, obesity, heart failure, and atrial stretch. Thus, our results provide a preclinical mechanistic basis rather than direct evidence of clinical efficacy, and caution is required when extrapolating to patients. Future studies should use models that better recapitulate chronic AF substrate development, such as long-term rapid atrial pacing, aged animals, or comorbidity-driven models incorporating hypertension, obesity, or heart failure to validate the therapeutic relevance of targeting the PIK3CA/TLR4 axis with PTX. Second, although gain- and loss-of-function experiments in AngII-stimulated HL-1 cardiomyocytes support a role for PTX via the PIK3CA/TLR4 axis, we did not perform *in vivo* genetic manipulation of these targets, which remains to be investigated. Finally, the sample size of human atrial tissues analyzed was limited, underscoring the need for larger clinical cohorts to validate these findings. Addressing these limitations will clarify the translational potential of PTX as an anti-ferroptotic intervention for AF.

6. Conclusions

This study integrates comprehensive bioinformatic analyses with *in vivo* validation to identify PIK3CA and TLR4 as principal molecular targets of PTX in the treatment of AF. Our findings demonstrate that PTX inhibits cardiomyocyte ferroptosis by modulating the PIK3CA/TLR4 signaling axis, thereby alleviating AF progression. These preclinical insights demonstrate the potential of PTX as a candidate anti-ferroptosis therapeutic and lay a preclinical foundation for the future development of targeted interventions for AF.

Availability of Data and Materials

The datasets utilized and analyzed in the current study are available from the corresponding author upon reasonable request.

Author Contributions

JBZ, ZYZ and FZ: Conceptualization, Methodology, Data Curation, Formal Analysis, Investigation, Validation, Writing – Original Draft. TPW, NZ and ZHS: Bioinformatics Analysis, Network Pharmacology, Data Interpretation, Software, Validation. HHL and YL: Experimental Validation, Animal Modeling, *In Vivo* Assays, Visualization. JXS and DW: Molecular Docking Analysis, scRNA-seq Data Processing, Visualization. YQY and WRW: Immunological Analysis, CIBERSORT Profiling, Correlation Studies. LLQ and RXW: Supervision, Conceptualization, Project Administration, Funding Acquisition, Resources, Writing – Review & Editing. All authors contributed to editorial changes in the manuscript. All authors read and approved the final manuscript. All authors have participated sufficiently in the work and agreed to be accountable for all aspects of the work.

Ethics Approval and Consent to Participate

The Animal Ethics Committee of Wuxi People's Hospital approved all experimental procedures (Approval number: DL2025016). All animal experimental procedures were conducted in strict accordance with the National Guidelines for Ethical Review of Laboratory Animal Welfare (GB/T 35892-2018) and relevant local regulations. The principles of the 3Rs (Replacement, Reduction, and Refinement) were strictly observed throughout the study, which was reported following the ARRIVE guidelines for animal research.

Acknowledgment

Not applicable.

Funding

This project was supported in part by the National Natural Science Foundation of China (82370342), the National Natural Science Foundation of China (82500408) and the Postgraduate Research & Practice Innovation Program of Jiangsu Province (SJCX24_0729).

Conflicts of Interest

The authors declare no conflicts of interest.

Supplementary Material

Supplementary material associated with this article can be found, in the online version, at https://doi.org/10.31083/FBL51871.

References

[1] Wijesurendra RS, Casadei B. Mechanisms of atrial fibrillation. Heart (British Cardiac Society). 2019; 105: 1860–1867. https://doi.org/10.1136/heartjnl-2018-314267

[2] Zimetbaum P. Atrial Fibrillation. Annals of Internal Medicine. 2017; 166: ITC33–ITC48. https://doi.org/10.7326/AITC201703070

[3] Komal S, Yin JJ, Wang SH, Huang CZ, Tao HL, Dong JZ, et al. MicroRNAs: Emerging biomarkers for atrial fibrillation. Journal of Cardiology. 2019; 74: 475–482. https://doi.org/10.1016/j.jjcc.2019.05.018

[4] Ma TL, Chen JX, Zhu P, Zhang CB, Zhou Y, Duan JX. Focus on ferroptosis regulation: Exploring novel mechanisms and applications of ferroptosis regulator. Life Sciences. 2022; 307: 120868. https://doi.org/10.1016/j.lfs.2022.120868

[5] Zheng J, Conrad M. The Metabolic Underpinnings of Ferroptosis. Cell Metabolism. 2020; 32: 920–937. https://doi.org/10.1016/j.cmet.2020.10.011

[6] Liu G, Xie X, Liao W, Chen S, Zhong R, Qin J, et al. Ferroptosis in cardiovascular disease. Biomedicine & Pharmacotherapy = Biomedecine & Pharmacotherapie. 2024; 170: 116057. https://doi.org/10.1016/j.biopha.2023.116057
[7] Ju H, Liu T, Yang M, Cheng M, Wu G. Iron and atrial fibrillation: A review. Pacing and Clinical Electrophysiology: PACE. 2023; 46: 312–318. https://doi.org/10.1111/pace.14678
[8] Yue H, Zhan Y, Zhang Z, Liang W, Wu Z. The emerging role of ferroptosis in myocardial fibrosis of atrial fibrillation. Archives of Medical Science: AMS. 2023; 19: 507–512. https://doi.org/10.5114/aoms/160941
[9] Brie D, Sahebkar A, Penson PE, Dinca M, Ursoniu S, Serban MC, et al. Effects of pentoxifylline on inflammatory markers and blood pressure: a systematic review and meta-analysis of randomized controlled trials. Journal of Hypertension. 2016; 34: 2318–2329. https://doi.org/10.1097/HJH.0000000000001086
[10] Siegel AN, Rodrigues N, Nasri F, Wilkialis L, Lipsitz O, Lee Y, et al. Novel therapeutic targets in mood disorders: Pentoxifylline (PTX) as a candidate treatment. Progress in Neuro-psychopharmacology & Biological Psychiatry. 2021; 104: 110032. https://doi.org/10.1016/j.pnpbp.2020.110032
[11] Black RS, Barclay LL, Nolan KA, Thaler HT, Hardiman ST, Blass JP. Pentoxifylline in cerebrovascular dementia. Journal of the American Geriatrics Society. 1992; 40: 237–244. https://doi.org/10.1111/j.1532-5415.1992.tb02075.x
[12] Ritchie ME, Phipson B, Wu D, Hu Y, Law CW, Shi W, et al. limma powers differential expression analyses for RNA-sequencing and microarray studies. Nucleic Acids Research. 2015; 43: e47. https://doi.org/10.1093/nar/gkv007
[13] Yu G, Wang LG, Han Y, He QY. clusterProfiler: an R package for comparing biological themes among gene clusters. Omics: a Journal of Integrative Biology. 2012; 16: 284–287. https://doi.org/10.1089/omi.2011.0118
[14] Zhou J, Xiong W, Wang Y, Guan J. Protein Function Prediction Based on PPI Networks: Network Reconstruction vs Edge Enrichment. Frontiers in Genetics. 2021; 12: 758131. https://doi.org/10.3389/fgene.2021.758131
[15] Chin CH, Chen SH, Wu HH, Ho CW, Ko MT, Lin CY. cytoHubba: identifying hub objects and sub-networks from complex interactome. BMC Systems Biology. 2014; 8: S11. https://doi.org/10.1186/1752-0509-8-S4-S11
[16] Ito K, Murphy D. Application of ggplot2 to Pharmacometric Graphics. CPT: Pharmacometrics & Systems Pharmacology. 2013; 2: e79. https://doi.org/10.1038/psp.2013.56
[17] Robin X, Turck N, Hainard A, Tiberti N, Lisacek F, Sanchez JC, et al. pROC: an open-source package for R and S+ to analyze and compare ROC curves. BMC Bioinformatics. 2011; 12: 77. https://doi.org/10.1186/1471-2105-12-77
[18] Qing J, Li C, Hu X, Song W, Tirichen H, Yaigoub H, et al. Differentiation of T Helper 17 Cells May Mediate the Abnormal Humoral Immunity in IgA Nephropathy and Inflammatory Bowel Disease Based on Shared Genetic Effects. Frontiers in Immunology. 2022; 13: 916934. https://doi.org/10.3389/fimmu.2022.916934
[19] Li J, Zhang Y, Lu T, Liang R, Wu Z, Liu M, et al. Identification of diagnostic genes for both Alzheimer's disease and Metabolic syndrome by the machine learning algorithm. Frontiers in Immunology. 2022; 13: 1037318. https://doi.org/10.3389/fimmu.2022.1037318
[20] Dutta S, Datta S. A rank-sum test for clustered data when the number of subjects in a group within a cluster is informative. Biometrics. 2016; 72: 432–440. https://doi.org/10.1111/biom.12447
[21] Pripp AH. Pearson's or Spearman's correlation coefficients. Tidsskrift for Den Norske Laegeforening: Tidsskrift for Praktisk Medicin, Ny Raekke. 2018; 138. https://doi.org/10.4045/tidsskr.18.0042 (In Norwegian)
[22] Lu Y, Tan L, Xie J, Cheng L, Wang X. Distinct microglia alternative splicing in Alzheimer's disease. Aging. 2022; 14: 6554–6566. https://doi.org/10.18632/aging.204223
[23] Trott O, Olson AJ. AutoDock Vina: improving the speed and accuracy of docking with a new scoring function, efficient optimization, and multithreading. Journal of Computational Chemistry. 2010; 31: 455–461. https://doi.org/10.1002/jcc.21334
[24] Seeliger D, de Groot BL. Ligand docking and binding site analysis with PyMOL and Autodock/Vina. Journal of Computer-aided Molecular Design. 2010; 24: 417–422. https://doi.org/10.1007/s10822-010-9352-6
[25] Hao Y, Stuart T, Kowalski MH, Choudhary S, Hoffman P, Hartman A, et al. Dictionary learning for integrative, multimodal and scalable single-cell analysis. Nature Biotechnology. 2024; 42: 293–304. https://doi.org/10.1038/s41587-023-01767-y
[26] Hänzelmann S, Castelo R, Guinney J. GSVA: gene set variation analysis for microarray and RNA-seq data. BMC Bioinformatics. 2013; 14: 7. https://doi.org/10.1186/1471-2105-14-7
[27] Jin S, Guerrero-Juarez CF, Zhang L, Chang I, Ramos R, Kuan CH, et al. Inference and analysis of cell-cell communication using CellChat. Nature Communications. 2021; 12: 1088. https://doi.org/10.1038/s41467-021-21246-9
[28] Trapnell C, Cacchiarelli D, Grimsby J, Pokharel P, Li S, Morse M, et al. The dynamics and regulators of cell fate decisions are revealed by pseudotemporal ordering of single cells. Nature Biotechnology. 2014; 32: 381–386. https://doi.org/10.1038/nbt.2859
[29] Shi S, Mao X, Lv J, Wang Y, Zhang X, Shou X, et al. Qi-Po-Sheng-Mai granule ameliorates Ach-$CaCl_2$ -induced atrial fibrillation by regulating calcium homeostasis in cardiomyocytes. Phytomedicine: International Journal of Phytotherapy and Phytopharmacology. 2023; 119: 155017. https://doi.org/10.1016/j.phymed.2023.155017
[30] Zhang X, Meng F, Song J, Zhang L, Wang J, Li D, et al. Pentoxifylline Ameliorates Cardiac Fibrosis, Pathological Hypertrophy, and Cardiac Dysfunction in Angiotensin II-induced Hypertensive Rats. Journal of Cardiovascular Pharmacology. 2016; 67: 76–85. https://doi.org/10.1097/FJC.0000000000000316
[31] Zhan Y, Zhou Y, Zhang C, Zhai Z, Yang Y, Liu X. Transferrin receptor knockdown attenuates atrial fibrillation by inhibiting cardiomyocyte ferroptosis and atrial fibrosis. Experimental Animals. 2025; 74: 348–361. https://doi.org/10.1538/expanim.24-0127
[32] Cooke JP, Sukhovershin RA. Novel Markers for Adverse Events in Atrial Fibrillation. Journal of the American College of Cardiology. 2018; 72: 734–737. https://doi.org/10.1016/j.jacc.2018.04.091
[33] Fan S, Hu Y, Shi J. Role of ferroptosis in atrial fibrillation: a review. Frontiers in Pharmacology. 2025; 16: 1362060. https://doi.org/10.3389/fphar.2025.1362060
[34] Morin GM, Zerbib L, Kaltenbach S, Fraissenon A, Balducci E, Asnafi V, et al. *PIK3CA*-Related Disorders: From Disease Mechanism to Evidence-Based Treatments. Annual Review of Genomics and Human Genetics. 2024; 25: 211–237. https://doi.org/10.1146/annurev-genom-121222-114518
[35] Sun H, Shao Y. Transcriptome analysis reveals key pathways that vary in patients with paroxysmal and persistent atrial fibrillation. Experimental and Therapeutic Medicine. 2021; 21: 571. https://doi.org/10.3892/etm.2021.10003
[36] Ezeani M, Prabhu S. PI3K(p110α) as a determinant and gene therapy for atrial enlargement in atrial fibrillation. Molecular and Cellular Biochemistry. 2023; 478: 471–490. https://doi.org/10.1007/s11010-022-04526-w
[37] Li TL, Zhu NN, Zhao MX, Sun J, Yin Z, Xie P, et al. Omentin-1 attenuates atrial fibrillation via Src/PI3K/Akt signaling-

mediated anti-fibrotic effects in cardiac fibroblasts. European Journal of Pharmacology. 2025; 996: 177588. https://doi.org/10.1016/j.ejphar.2025.177588
[38] Bass-Stringer S, Bernardo BC, Yildiz GS, Matsumoto A, Kiriazis H, Harmawan CA, et al. Reduced PI3K(p110α) induces atrial myopathy, and PI3K-related lipids are dysregulated in athletes with atrial fibrillation. Journal of Sport and Health Science. 2025; 14: 101023. https://doi.org/10.1016/j.jshs.2025.101023
[39] Sun L, Wang H, Xu D, Yu S, Zhang L, Li X. Lapatinib induces mitochondrial dysfunction to enhance oxidative stress and ferroptosis in doxorubicin-induced cardiomyocytes via inhibition of PI3K/AKT signaling pathway. Bioengineered. 2022; 13: 48–60. https://doi.org/10.1080/21655979.2021.2004980
[40] Xiao Y, Yu Y, Hu L, Yang Y, Yuan Y, Zhang W, et al. Matrine Alleviates Sepsis-Induced Myocardial Injury by Inhibiting Ferroptosis and Apoptosis. Inflammation. 2023; 46: 1684–1696. https://doi.org/10.1007/s10753-023-01833-2
[41] Ye T, Yang W, Gao T, Yu X, Chen T, Yang Y, et al. Trastuzumab-induced cardiomyopathy via ferroptosis-mediated mitochondrial dysfunction. Free Radical Biology & Medicine. 2023; 206: 143–161. https://doi.org/10.1016/j.freeradbiomed.2023.06.019
[42] Wang Z, Dang T, Liu T, Chen S, Li L, Huang S, et al. NEDD4L Protein Catalyzes Ubiquitination of PIK3CA Protein and Regulates PI3K-AKT Signaling. The Journal of Biological Chemistry. 2016; 291: 17467–17477. https://doi.org/10.1074/jbc.M116.726083
[43] Wang Z, Liu Y, Huang S, Fang M. TRAF6 interacts with and ubiquitinates PIK3CA to enhance PI3K activation. FEBS Letters. 2018; 592: 1882–1892. https://doi.org/10.1002/1873-3468.13080
[44] Jin L, Hou P. Yixin-Fumai granules modulate autophagy through the PI3K/AKT/FOXO pathway and lead to amelioration of aging mice with sick sinus syndrome. Immunity & Ageing: i & a. 2024; 21: 46. https://doi.org/10.1186/s12979-024-00439-y
[45] Wei YR, Hou YL, Yin YJ, Li Z, Liu Y, Han NX, et al. Tongxinluo Activates PI3K/AKT Signaling Pathway to Inhibit Endothelial Mesenchymal Transition and Attenuate Myocardial Fibrosis after Ischemia-Reperfusion in Mice. Chinese Journal of Integrative Medicine. 2024; 30: 608–615. https://doi.org/10.1007/s11655-024-3652-5
[46] Dhulqarnain AO, Takzaree N, Hassanzadeh G, Tooli H, Malekzadeh M, Khanmohammadi N, et al. Pentoxifylline improves the survival of spermatogenic cells via oxidative stress suppression and upregulation of PI3K/AKT pathway in mouse model of testicular torsion-detorsion. Heliyon. 2021; 7: e06868. https://doi.org/10.1016/j.heliyon.2021.e06868
[47] Wei J, Yu L, Liu Y, Ye S, Song B, Deng Y, et al. Relationship between the expression of striated preferentially expressed gene (*SPEG*) and the development of atrial fibrillation. Journal of Thoracic Disease. 2025; 17: 1723–1735. https://doi.org/10.21037/jtd-2025-456
[48] Su Y, Ye Z, Hou J, Lin X, Zheng C, Xu L, et al. Identification of key genes and immune mechanisms in atrial fibrillation: An observational bioinformatics and single-cell transcriptome study. Medicine. 2026; 105: e48505. https://doi.org/10.1097/MD.0000000000048505
[49] Liang Y, Zhou Y, Wang J, He Y. Downregulation of fibromodulin attenuates inflammatory signaling and atrial fibrosis in spontaneously hypertensive rats with atrial fibrillation via inhibiting TLR4/NLRP3 signaling pathway. Immunity, Inflammation and Disease. 2023; 11: e1003. https://doi.org/10.1002/iid3.1003
[50] Gurses KM, Kocyigit D, Yalcin MU, Canpinar H, Yorgun H, Sahiner ML, et al. Monocyte Toll-Like Receptor Expression in Patients With Atrial Fibrillation. The American Journal of Cardiology. 2016; 117: 1463–1467. https://doi.org/10.1016/j.amjcard.2016.02.014
[51] Shuai W, Kong B, Fu H, Shen C, Jiang X, Huang H. MD1 Deficiency Promotes Inflammatory Atrial Remodelling Induced by High-Fat Diets. The Canadian Journal of Cardiology. 2019; 35: 208–216. https://doi.org/10.1016/j.cjca.2018.11.020
[52] Kong B, Fu H, Xiao Z, Zhou Y, Shuai W, Huang H. Gut Microbiota Dysbiosis Induced by a High-Fat Diet Increases Susceptibility to Atrial Fibrillation. The Canadian Journal of Cardiology. 2022; 38: 1962–1975. https://doi.org/10.1016/j.cjca.2022.08.231
[53] Lei G, Zhang Y, Hong T, Zhang X, Liu X, Mao C, et al. Ferroptosis as a mechanism to mediate p53 function in tumor radiosensitivity. Oncogene. 2021; 40: 3533–3547. https://doi.org/10.1038/s41388-021-01790-w
[54] Feng L, Cheng P, Feng Z, Zhang X. Transmembrane p24 trafficking protein 2 regulates inflammation through the TLR4/NF-κB signaling pathway in lung adenocarcinoma. World Journal of Surgical Oncology. 2022; 20: 32. https://doi.org/10.1186/s12957-021-02477-y
[55] Chen D, Geng Y, Deng Z, Li P, Xue S, Xu T, et al. Inhibition of TLR4 Alleviates Heat Stroke-Induced Cardiomyocyte Injury by Down-Regulating Inflammation and Ferroptosis. Molecules (Basel, Switzerland). 2023; 28: 2297. https://doi.org/10.3390/molecules28052297
[56] Xie SS, Deng Y, Guo SL, Li JQ, Zhou YC, Liao J, et al. Endothelial cell ferroptosis mediates monocrotaline-induced pulmonary hypertension in rats by modulating NLRP3 inflammasome activation. Scientific Reports. 2022; 12: 3056. https://doi.org/10.1038/s41598-022-06848-7
[57] Xiao Z, Kong B, Fang J, Qin T, Dai C, Shuai W, et al. Ferrostatin-1 alleviates lipopolysaccharide-induced cardiac dysfunction. Bioengineered. 2021; 12: 9367–9376. https://doi.org/10.1080/21655979.2021.2001913
[58] Carneiro PP, Dórea AS, Oliveira WN, Guimarães LH, Brodskyn C, Carvalho EM, et al. Blockade of TLR2 and TLR4 Attenuates Inflammatory Response and Parasite Load in Cutaneous Leishmaniasis. Frontiers in Immunology. 2021; 12: 706510. https://doi.org/10.3389/fimmu.2021.706510
[59] Xia DY, Zhang HS, Wu LY, Zhang XS, Zhou ML, Hang CH. Pentoxifylline Alleviates Early Brain Injury After Experimental Subarachnoid Hemorrhage in Rats: Possibly via Inhibiting TLR 4/NF-κB Signaling Pathway. Neurochemical Research. 2017; 42: 963–974. https://doi.org/10.1007/s11064-016-2129-0
[60] Al-Kharashi L, Attia H, Alsaffi A, Almasri T, Arafa M, Hasan I, et al. Pentoxifylline and thiamine ameliorate rhabdomyolysis-induced acute kidney injury in rats via suppressing TLR4/NF-κB and NLRP-3/caspase-1/gasdermin mediated-pyroptosis. Toxicology and Applied Pharmacology. 2023; 461: 116387. https://doi.org/10.1016/j.taap.2023.116387
[61] Liao CH, Akazawa H, Tamagawa M, Ito K, Yasuda N, Kudo Y, et al. Cardiac mast cells cause atrial fibrillation through PDGF-A-mediated fibrosis in pressure-overloaded mouse hearts. The Journal of Clinical Investigation. 2010; 120: 242–253. https://doi.org/10.1172/JCI39942
[62] Uemura K, Kondo H, Ishii Y, Kobukata M, Haraguchi M, Imamura T, et al. Mast Cells Play an Important Role in the Pathogenesis of Hyperglycemia-Induced Atrial Fibrillation. Journal of Cardiovascular Electrophysiology. 2016; 27: 981–989. https://doi.org/10.1111/jce.12995
[63] Hulsmans M, Schloss MJ, Lee IH, Bapat A, Iwamoto Y, Vinegoni C, et al. Recruited macrophages elicit atrial fibrillation. Science (New York, N.Y.). 2023; 381: 231–239. https://doi.org/10.1126/science.abq3061
[64] Suzuki A, Fukuzawa K, Yamashita T, Yoshida A, Sasaki N, Emoto T, et al. Circulating intermediate CD14++CD16+monocytes are increased in patients with

atrial fibrillation and reflect the functional remodelling of the left atrium. Europace: European Pacing, Arrhythmias, and Cardiac Electrophysiology: Journal of the Working Groups on Cardiac Pacing, Arrhythmias, and Cardiac Cellular Electrophysiology of the European Society of Cardiology. 2017; 19: 40–47. https://doi.org/10.1093/europace/euv422

[65] He L, Liu R, Yue H, Zhang X, Pan X, Sun Y, et al. Interaction between neutrophil extracellular traps and cardiomyocytes contributes to atrial fibrillation progression. Signal Transduction and Targeted Therapy. 2023; 8: 279. https://doi.org/10.1038/s41392-023-01497-2

[66] Natorska J, Ząbczyk M, Undas A. Neutrophil extracellular traps (NETs) in cardiovascular diseases: From molecular mechanisms to therapeutic interventions. Kardiologia Polska. 2023; 81: 1205–1216. https://doi.org/10.33963/v.kp.98520